Towards quantifying the intracellular trafficking of silk nanoparticles in cancer cells: Establishing biomarkers in the laboratory setting for the characterisation of subcellular fractions

By

Samuel G. Huff Guelbert

Declaration of authenticity and author's rights

'This thesis is the result of the author's original research. It has been composed by the author and has not been previously submitted for examination which has led to the award of a degree.'

Signed:

Date:

Acknowledgements

This thesis is the culmination of a number of years work, and while it represents my research and a personal achievement, it also stands as a testament to the continued, unwavering support and guidance of those around me.

First and foremost I would like to thank Dr Philipp Seib with whose careful direction and support all laboratory work was undertaken and the many iterations of the thesis were written. I would also like to thank Prof. Clive Wilson for his support in the undertaking of this work as well.

Secondly, I extend my thanks to my family, Richard, Annalise, Jacob and Bethany, for their untiring assistance and encouragement throughout my academic career and especially in the support they gave in the creation of this thesis.

Of course, special thanks must also be given to the many good friends who supported me for their company and many entertaining diversions.

My deepest gratitude also to:

Edward Devlin

James Edmond

Kelly Etherson

Laura Flemming

James Judge

David Mallinson

Abstract

Silk has emerged as a promising contender for drug delivery applications, including the use of silk nanoparticles for anticancer drug delivery. Nanoparticles are internalised into cells via endocytosis; thus, silk nanoparticles have been proposed for lysosomotropic drug delivery. However, the intracellular fate of these nanoparticles has not been documented. One approach for quantifying the intracellular fate of silk nanoparticles is subcellular fractionation. Adequate, but gentle, homogenisation of cells, followed by characterisation of the subcellular fractions using biochemical markers, are key requirements for quantitative trafficking studies. Therefore, the aim of this thesis was to develop wet-lab tested biochemical marker assays for B16F10 cell subcellular fractions.

The following biochemical marker assays were first scaled and refined: alkaline phosphatase to assay for the plasma membrane, succinate dehydrogenase for mitochondria, lactate dehydrogenase for the cytosol, N-acetyl-ß-glucosaminidase for lysosomes and DNA for the nucleus. A homogenisation scheme was then developed, using a cell cracker with 7 μm clearance. At four passes, this device provided over 80% ± 15 cell breakage, while retaining high lysosomal latency (82% ± 1 3.6), thereby providing a sample representative of the whole cell population.

Trafficking studies require the use of non-toxic nanoparticle concentrations; therefore, silk nanoparticles were assessed for cytotoxicity in B16F10 cells using an MTT assay. The IC_{50} of silk nanoparticles was 17.58 μg/ml, using dextran (IC_{50} >200 μg/ml) and PEI (IC_{50} 8.8 μg/ml) as negative and positive controls, respectively. These silk nanoparticles had a 131 nm diameter, with a polydispersity of 0.2, and a zeta potential in distilled water of -34.6 mV, as characterised by dynamic light scattering and zeta potential measurements, respectively.

In conclusion, this thesis lays the groundwork for subsequent performance of wet-lab biomarker assays on subcellular fractions to quantify the intracellular trafficking of silk nanoparticles.

Contents

1 Introduction

There has been considerable recent effort to advance silk as a viable material for nano-scale drug delivery (1–4), with the creation and administration of drug adsorbed silk nanoparticles (5). These nanoparticles have proven extremely effective at both carrying and releasing drugs in response to cellular stimuli (e.g. pH, enzyme activity) (3), and exploiting the enhanced permeation and retention effect in order to deliver drugs precisely to the tumour microenvironment (6), where they are often endocytosed through a variety of pathways (7). Following intravenous dosing with silk nanoparticles it seems feasible that these silk nanoparticles can accumulate in solid tumours due to the tumour's leaky blood vessels and reduced lymphatic drainage; indeed this pathophysiology has been widely exploited when designing macromolecular drug carriers for solid tumour targeting (6). Once in the tumour tissue, silk nanoparticles are expected to gain access into tumour cells though the process of endocytosis (7). It is vital to gain an understanding of the intracellular fate of these nanoparticles in order to better ensure delivery to their site of activity. However, to date, this remains unknown. There are a number of methods of tracing the fate of such nanoparticles, including fluorescence microscopy and subcellular fractionation. Only fractionation provides us with truly quantitative method of evaluating the distribution of nanoparticles in cells (8). Subcellular fractionation requires great precision and the establishment of biomarker assays to correctly identify and interrogate subcellular fractions for the presence of silk nanoparticles (9). To fully understand the scope of this thesis it

is important to have a basic background knowledge of endocytosis (Section 1.4), subcellular fractionation (Sections 1.5 – 1.7) and silk (Section 1.1).

1.1 Silk as a biomaterial

The biopolymer silk has long been used in medical applications, finding use in sutures, dressings and more recently on a smaller scale, being used in scaffolds for controlled drug release (10) and nanoparticles (11). The excellent mechanical and biological properties of silk have been instrumental in seeing it used in a medical setting (12), its biocompatibility chief among them and its highly crystalline structure following preparation and removal of its amorphous regions (13) allowing it to retain a large degree of mechanical strength, and still remain tightly controllable. Silk is still regularly used in modern medicine; however, more recently it is finding more advanced purposes than simple sutures.

Silk is widely examined for, among many other applications, drug delivery (Table 1.1). It is highly controllable and is typically regarded to possess excellent biocompatibility (14) making silk an excellent candidate for a cheap, highly scalable, versatile and controllable drug delivery system which can be generated under aqueous conditions (5). It has been used to deliver a wide range of therapeutics including genes(15) , small molecular weight drugs (16), and cytotoxic chemotherapeutic drugs (5).

Table 1.1 Recent Drug release studies using silk fibroin based drug delivery methods.

Form	Delivery method	Molecule delivered	Model used	Delivery duration	Reference
Hydrogel	Implantation into the maxillary sinus floor	$VEGF_{165}$ BMP-2	Rabbit	28 Days	(17)
Nanoparticles	Intraperitoneal injection	Paclitaxel	Mouse	13 Days	(18)
Porous scaffold	Subcutaneous implantation	BMP-2	Mouse	5 weeks	(2)
	Subcutaneous implantation	rhBMP-2	Rat	21 days	(19)
Microneedles	Subcutaneous implantation	Imaging agents (DiD, Alexa Flour-488)	C57BL/6 mice	15+ days	(20)
Micro particles		rhBMP-2 rhIGF-1 HRP	Human mesenchymal stem cells	5 weeks	(21)

One of the key challenges faced by conventional, low molecular weight, chemotherapeutic agents is their poor pharmacokinetics, i.e. the absence of effective targeting to the site of required action (22). Furthermore, these drugs are often poorly water soluble (22) or induce undesirable side effects, such as myocardial ischemia (23), both of which are limiting factors on their dosing. For example, anthracyclines exhibit cumulative cardiotoxicity (24), resulting in a maximum cumulative dosage in the clinical setting in the absence of effective tumour targeting.

Therefore target drug delivery to the tumour microenvironment is one potential avenue to improve clinical response (and potentially increase dosing). It is well established that angiogenesis in a tumour results in poorly structured and leaky vasculature which can be exploited for targeted drug delivery (25). One method of exploiting this pathology is to design nanoparticles to target this tumour microenvironment.

Nanoparticles have in general, have been shown to have highly controllable drug release profiles and are able to be tailored towards stimuli-responsive release, specifically pH which is useful when targeting intracellular compartments such as lysosomes and late endosomes (17). This controllability can also be exploited for silk-based system where drug release ranging from extended time frames to very shorter timespan can be engineered into the system (5). Furthermore, silk is amenable to in process controls such as size, crystallinity, and drug content (3).

As such it is important to have a robust understanding of the structure of silk and its properties in order to gain an appreciation of its development and behaviour as a drug carrier.

1.2 Structure and properties of silk

Silk spun by the silkworm *B. mori* is a natural biopolymer comprising two types of fibre; silk fibroin and silk sericin (Fig 1.1), the latter being the gumming agent for the cocoon which is typically removed due to its propensity to induce an inflammatory response(26).

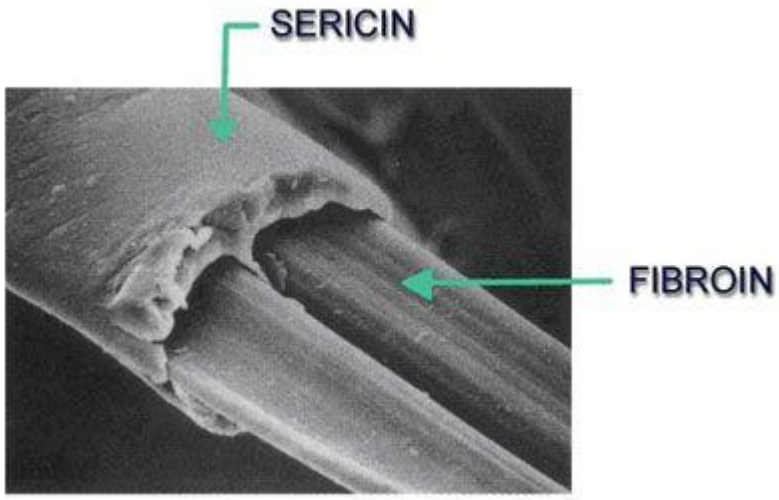

Fig 1.1. The microstructure of *B. mori* silk as imaged using scanning electron microscope (SEM). (27)

B. mori silk fibroin consists of a hydrophobic heavy chain (~390 kDa) and a light chain (~25 kDa), that are linked by one disulphide bond, and which are present in an equimolar ratio (28). The raw silk then consists of a parallel arrangement of the light and heavy chains which are joined together at the C-terminus of the heavy chain forming a complex of the two chains (Fig 1.2) (29) which are then sheathed with a layer of sericin, a protein which acts as a gumming agent and adds structural stability to the final construct (30).

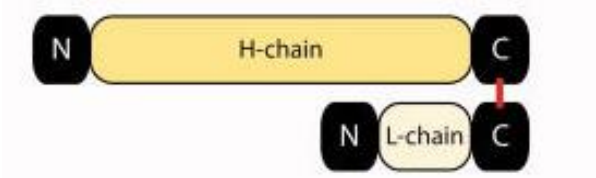

Fig 1.2 The arrangement of the heavy and light chains in *B. mori* silk fibroin. (31)

The heavy chain consists of 12 low complexity crystalline domains, which exhibit high proportions of a 'GX' or glycine-X dipeptide repeat where 'X' represents alanine in 65% of the 'GX' repeats, serine in 23%, tyrosine in 9% of the repeats and predominantly valine in the other 3% with only 4.7% of the remaining amino acids being used. This 'GX' repeat is the main structural component of the β-sheets present in the heavy chain of silk fibroin (32). This allows one face of the β-sheet to present only glycine residues, suggesting tight glycine-glycine packaging and the other face to present larger side chains in the case of tyrosine, a large number of hydroxyl groups in the case of serine and a carboxyl group on alanine residues (33). The placement and arrangement of these groups allow hydrogen bonding to occur in the secondary structure of silk, contributing to some of the mechanical properties for which silk is so well known, including its tensile strength.

The crystalline regions are interspersed with the tetrapeptide GAAS (Gly-Ala-Ala-Ser). The GAAS tetrapeptide is instrumental in making the transition between silk I and silk II. During the process of spinning the cocoon, the GAAS repeat encourages the transformation from β-twist to β-sheet structures through conformational changes induced around the α and β carbon atoms in the alanine residues (34). These highly crystalline structures have been found to measure 0.7 nm along the

fibre's axis, be spaced between 0.93 nm to 1.57 nm and evenly dispersed within the whole silk matrix (35).

These GX repeats and GAAS tetrapeptides are found in 12 domains connected with short 'linker' domains. These linker domains are characterised by their non-repetitive amorphous composition (32) and hydrophilicity (36), in contrast to the more crystalline regions hydrophobicity (37). Such amorphous linker domains are noted to lend silk its physical flexibility and malleability where water plays the role of a plasticiser in the amorphous linker regions (38). This combination of highly crystalline and amorphous regions allows silk to maintain high mechanical strength while also exhibiting great flexibility and variety in its applications.

The light chain of silk fibroin is a chain of ~25 kDa, and is linked to the heavy chain by a single disulphide bond at the C terminus of each peptide chain and exhibits a non-repetitive sequence, but otherwise plays only a marginal role in the properties of the silk fibre itself (32). The heavy chain and light chain together form the fibres of silk fibroin in an equimolar ratio (28,39), which are organised and held together by a third protein, silk sericin.

Silk sericin is a glue-like protein which comprises around 25 to 30 % of the silk cocoon, and consists of 18 amino acids most of which have strongly polar R groups (40), including carboxyl, hydroxyl, and amino groups. Sericin is characterised by a high serine content (roughly 30 %) (41). Sericin presents most frequently as a random coil but occasionally with a high β-sheet content (39). The role of sericins

in silk fibre and the structures they comprise is primarily as a gumming agent. Principally this allows the bundled silk fibres to retain their structural integrity when used in cocoons and also provides limited protection for the fibroin from damage.

Silk fibroin can take one of three forms; silk I, silk II and silk III. The transition between these states is usually irreversible without further treatment of the silk and follows a transition from a less stable to a more stable form, in the presence of the correct conditions. This transformation of the tertiary structure of silk allows arthropods to spin the water soluble silk I and then await the transformation into silk II, the insoluble and tougher, more crystalline form of silk (42).

Silk I is relatively unstable and water soluble, and is the form in which silk resides in the silk glands before it is spun by *B. mori*. It has a high ß-turn content combined with greater amorphous regions than silk II, as confirmed by X-ray diffraction (43,44) and nuclear magnetic resonance (NMR) (43). The β-turn structures present in silk I are also of the appropriate length to form into antiparallel strands forming the β-sheet structures which characterise the silk II form (43).

Silk I may easily be converted into silk II via a process hypothesised to rely upon nucleation dependent aggregation in the presence of water (45). In such cases, the presence of water is vital, as a more swollen fibre will offer greater room for the peptide chains to move and change their conformation (42).

Silk II, the spun form of silk, concurrently has a highly crystalline structure, being rich in pleated ß-sheets. It is during the formation of these ß-sheets that water is forced from the hydrophobic regions of the silk, contributing to the stability of form II (36). This is hypothesised to occur during spinning as the β-sheet regions in silk I serve as a nucleus for the formation of silk II (43). Silk II is also insoluble in water and exhibits the tightly packed and uniformly dispersed β-sheets seen in silk fibroin (32). It is silk II which forms the cocoon of *B. mori* and serves as the primary state of silk in most manufacturing, due to its tensile strength and tight controllability. However, for most biological applications, it is necessary to reprocess the silk back to a less crystalline form in order to take advantage of silk's highly malleable nature when exhibiting a high proportion of amorphous domains (16).

Silk III has a hexagonal, left-handed, threefold helical structure, which separates the serine and alanine residues creating a hydrophobic column(46). This form of silk was first discovered at the aqueous fibroin-organic solvent interface and can also be found at the air-water interface and exhibits surfactant properties (47). Silk III however is rarely found during processing into nanoparticles and is not currently under investigation as a potential biomaterial for a drug carrier.

The most stable form is silk II, which comprises mostly pleated ß-sheets in a more extended manner and thus has a higher stability and controllability than silk I. This is due chiefly to, that in the transition from silk I to silk II, the amorphous regions

undergo a transition between β-twists to β-sheets, a transition from a less stable to a more stable secondary structure (34,36,37). This confers greater molecular stability and thus it is possible to more precisely manipulate silk II during manufacturing due to the greater predictability of the conformational changes during the transformation process and the higher crystallinity of silk II.

All of these properties make silk a highly desirable biomaterial for drug delivery. The crystallinity of silk can be fine-tuned when producing nanoparticles (5), scaffolds (2) and microneedle arrays (4) for drug delivery as outlined in table 1.1. For example, the polar natures of these crystalline and amorphous regions allow adsorption of drugs (5)to the surface of these particles and within the interior of scaffolds. It also allows drugs to be either conjugated to the silk fibres themselves or drugs to be encapsulated within the particles during manufacturing (48).

Silk is usually processed in a regenerative manner, breaking down the raw material often using lithium salts, and regenerating the silk from an aqueous solution (49). The starting material for this process is often silk II, having already been spun by *B. mori*, it is necessary to process the silk to achieve the controllability desired. This process renders a form of silk very similar to silk I, and allows regeneration into a nanoparticle of the required size, shape and composition.

In order to be made suitable for any medical applications, the silk sericin protein must be removed from the cocoons due to its propensity to invoke an inflammatory response. This inflammatory response is driven primarily by the antigenic activity of sericin (50,51) when implanted in vivo or applied to a cell culture (52). It is thus desirable to remove completely the sericin natively present in silk before reprocessing it into a viable drug carrier suitable for clinical use.

In vivo, silk fibroin is degraded into non-toxic products along existing proteolytic pathways at a predictable rate (53). Proteases have been demonstrated to cleave silk non-discriminately (54), facilitating quick release of the adsorbed drugs and preventing the accumulation of silk nanoparticles in the body.

As such, silk remains a prime candidate for drug delivery applications over similar synthetic materials such as silica for example (55).

1.3 Nanomedicine development in a clinical setting

While silk is a highly desirable biomaterial, it is by no means the only material being explored in this capacity. There are currently a large number of other nanoparticle-based drug carriers under significant study which are approaching clinical use and some which already see routine use in the healthcare sector (summarised in Table 1.2). The most commonly used and thus well-known is doxorubicin loaded PEGylated liposomes which have been noted to reduce cardiotoxicity in patients in comparison to unmodified doxorubicin (56). Alongside PEG, various other approaches are being used, such as drug conjugates like paclitaxel poliglumex (PPX), albumin nanoparticles (abraxane), the antibody-drug conjugate Adcetris, and even inorganic iron oxide nanoparticles (NanoTherm). All of these are currently seeing clinical use in some capacity. The advantages of these nanoparticles are many, however they are still prone to very similar problems, such as accumulation to toxic levels in the case of iron oxide nanoparticles (57,58), toxicity of the carrier itself in the case of quantum dots (59), or even promoting immune responses in the case of PEGylated liposomes, which often produce an IgM response (60).

Nanoparticles have drawn such attention due to their proven utility in a laboratory setting. Initially, Doxil, a liposomal polyethylene glycol (PEG) stabilised liposome loaded with doxorubicin, was approved for human clinical use in 1995 being one of the first anti-cancer nanomedicines available (61). The swift approval of further

liposomal nanomedicines such as a liposomal form of daunorubicin, DaunoXome (62), also in 1995, and more recently liposomal irinotecan (Onivyde) (63)by the Food and Drug Administration (FDA) in the US is hardly surprising given their proven utility. To date however, the protein-bound paclitaxel nanoparticle Abraxane is the only non-liposomal nanoparticle approved by the FDA for human use (64).

Table 1.2. Nanoparticles approaching or currently in clinical use. Adapted from (65).

Type of carrier	Drug	Status	Application	Reference
Polymer-drug conjugates	**Paclitaxel**			
	Paclitaxel poliglumex (PPX)	Phase III clinical trials.	Ovarian cancer.	(66)
Liposomes	**Doxorubicin**			
	Doxil	Clinical use.	Ovarian cancer.	(67)
	Lipo-Dox	Clinical use.	Breast/ovarian cancer.	(56) (68)
	Myocet	Clinical use.	Breast cancer.	(67)
	Caelyx	Clinical use.	Breast/ovarian cancer.	
	Daunorubicin			(69)
	DaunoXome	Clinical use.	Karposi's sarcoma.	
	Cisplatin			(70)
	LipoPlatin	Phase III clinical trials.	Non-small cell lung cancer.	
Inorganic compounds	**Iron oxide**			
	Venofer (Iron sucrose)	Clinical use.	Anemia.	(71)
Antibody-drug conjugates	**Emtansine/trastuzumab**			
	Kadcyla	Clinical use.	Breast cancer.	(72)
	Brentuximab/vedotin			
	Adcetris	Clinical use.	CD30 Lymphoma.	(73)

Recently, silk nanoparticles have emerged as a promising contender for drug delivery. The ease of production of silk nanoparticles is unique They can be produced in ambient conditions (5) using comparatively mild aqueous solutions(74).

Additionally of silk is regarded as biocompatible and an FDA approved biomaterial for use in humans. As a well-established biomaterial, we have an appreciable understanding of silk's biomechanical properties and how these may be exploited to render different release profiles for adsorbed drugs (5), as well as the physical characteristics of the nanoparticles themselves (3,75). It is therefore expected that silk can be easily broken down inside the lysosome which allows us to avoid issues typically encountered with inorganic carrier such as iron oxide nanoparticles (58,76) and quantum dots (59).

Lastly, it is important to consider the toxicity of the carrier itself. Silk has demonstrated high biocompatibility and once processed appropriately, it elicits minimal immune response (11).

Though these properties render an effective method of drug delivery, they are impotent unless the materials can be correctly introduced to the area of the body in which they are needed, or function with the greatest efficacy. The only way silk nanoparticles may enter a cell and release its payload is via endocytosis. It is therefore necessary to have a basic understanding of both targeting towards the

tumour microenvironment and endocytosis including the possible paths into a cell silk nanoparticles may take.

1.4 Endocytosis and intracellular trafficking

When considering intracellular trafficking, it is important to have a good understanding of the mechanisms by which drug delivery systems can be internalised into a cell and the effect that this has on their final fate.

When targeting nanoparticles towards the tumour microenvironment we may exploit a phenomenon known as the enhanced permeation and retention effect (EPR effect) (6). During angiogenesis in a tumour of volume greater than $1mm^3$, it is observable that the vasculature is poorly formed and leaks into the surrounding tissue and lymphatic drainage is poor (Fig 1.3). This pathophysiology is easily exploited by the application of nanoparticle drug carriers which can fit through these gaps in the vasculature and can then passively accumulate in the extracellular space in a higher concentration than would normally be seen in healthy tissue and indeed in the low molecular weight payload itself (77). This passive accumulation of nanoparticles allows tumour targeting of solid tumour and changes the uptake mechanism of a low molecular weight payloads from passive diffusion across the plasma membrane to an endocytic uptake mechanism. This now provides opportunities to overcome drug resistance mechanisms often seen with low molecular weight chemotherapetuic agents; here plasma membrane pumps render passive diffusion of the chemotherapeutic agents ineffective (78).
Upon endocytic uptake, the nanoparticles are taken into the lysosomal pathway and broken down releasing the adsorbed drug internally (48).

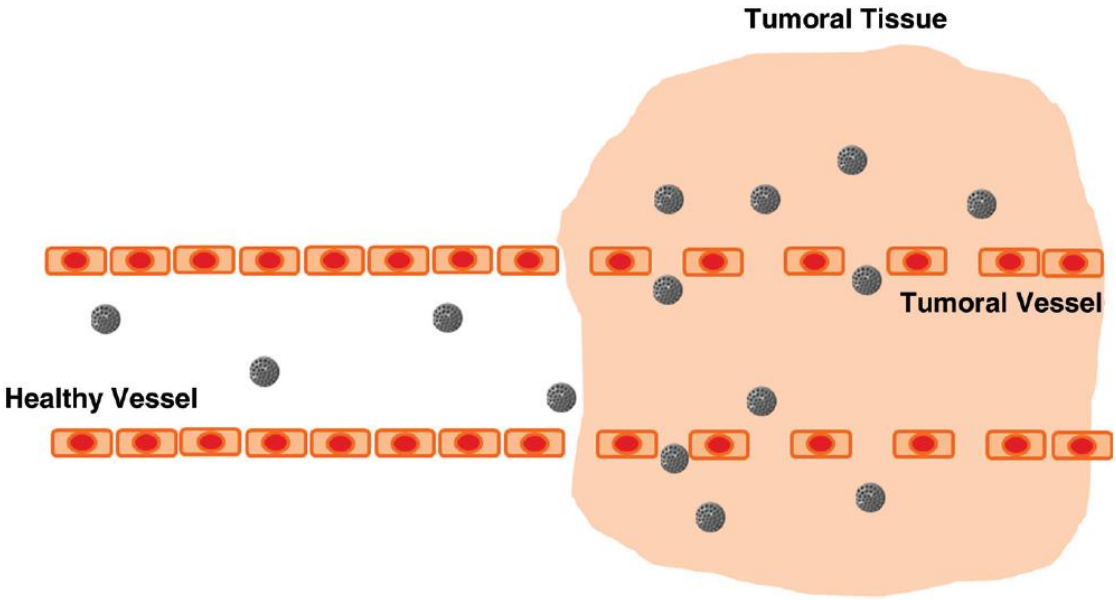

Fig: 1.3 The basis of the EPR effect as a therapeutic agent moves from leaky vasculature to the tumour microenvironment. (55)

Endocytosis, far from being simply a method of cellular uptake, governs a plethora of cellular processes including, but not limited to, neurotransmission (79), extracellular communication (80), mediating immune responses (81) and cellular secretion (82).

Playing such a vital role in cellular regulation, endocytosis is a highly regulated process. Although exocytosis and secretion have no role in nanomedicine uptake, they play a vital role in mediating residence time within the cell, being one of the largest sinks for the intracellular milieu. It is the constitutive uptake by these cells that we exploit when applying nanoparticles to cells with a view to internalisation.

During endocytosis, the plasma membrane becomes invaginated, and eventually closes around itself and moves into the internal cellular environment.

From this point there are a number of pathways to follow depending on the type of endocytosis (Fig 1.4) however, it is not intended to cover regulation here, only examine endocytosis in the context of drug delivery. A number of reviews cover endocytosis and exocytosis regulation in great detail (83) (84) both covering large areas of regulation and the effect this has on trafficking.

Endocytosis can be segregated into three main pathway types. The first, fluid phase endocytosis refers to the endocytosis of solutes in the immediate environment of the cell in a nonspecific manner, and in the concentration they are found in their solvent (85). In contrast, both absorptive and receptor-mediated endocytosis require binding of molecules to receptor molecules on the cell surface membrane, adding specificity to the process and somewhat concentrating the molecules before endocytosing them (86). This may also allow other particles to exploit a premade invagination and endocytic instance in what is known as 'piggyback endocytosis' and they are included in the invagination in a similar fashion to fluid phase internalisation.

Larger particulate matter optimised particles and nanoparticles are taken up via phagocytosis (87). Following complete invagination, the early structure now dubbed a phagosome can mature to a late endosome and subsequently a lysosome.

This pathway is easily exploited by a previous study on silk nanoparticles in particular, where a large aggregation was to be found in late endosomes and lysosomal structures (5).

Endocytic openings may be between 50 to hundreds of nm in diameter. The two most prevalent are clathrin mediated and caveolae mediate pinocytosis, with macropinocytosis being less common, but no less important.

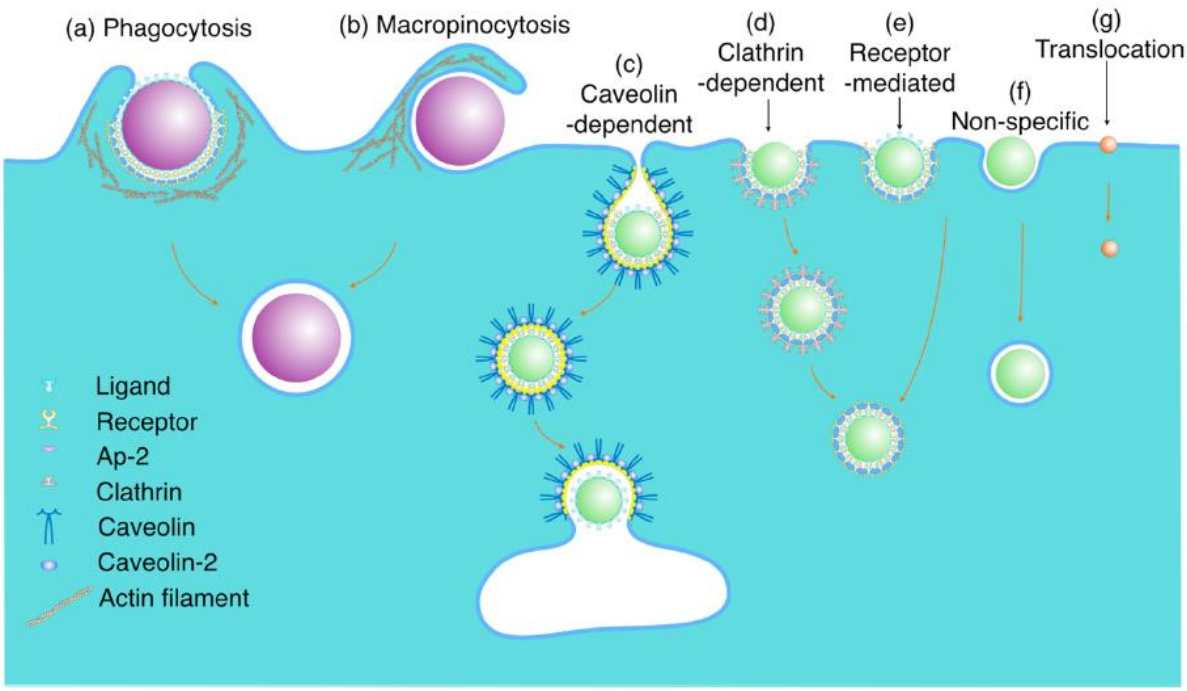

Figure 1.4. The various endocytic routes into the cell open to exploitation by nano scale therapeutics. (7)

Clathrin-mediated endocytosis (Fig 1.4 d) is the best characterised of all the endocytic pathways. Clathrin mediation by way of adaptor proteins linking the

clathrin to the plasma membrane will initiate the pinocytosis of particles and extracellular fluid. It is debated exactly how this is initiated, with the prevailing theory being that the AP2 complex initiates the reaction by way of recruiting clathrin molecules to the plasma membrane (88). This process occurs constitutively facilitating nutrient and growth factor uptake (89).

The first stage of clathrin mediated endocytosis is the binding of a ligand to the surface of the cell and the recruitment of further receptors, resulting in the concentration of receptors in an invaginated pit. The pit then the pinches off from the membrane and is fully internalised (87,90,91). Following internalisation the endosome will either cycle back with its contents to the cell membrane to maintain cellular homoeostasis. They may also be trafficked further into the endosomal pathway and mature into a late endosome and later a lysosome through a gradual decrease in pH, for degradation or use (92). It should be noted that the recycling of endosomes back to the membrane immediately does not constitute effective drug delivery.

Though clathrin mediated endocytosis is one gateway into the cell there are a number of other parallel mechanisms, for example caveolae dependent uptake, which are involved in internalising extracellular constituents.

Caveolae are small, flask-shaped invaginations in the cell membrane present in many cell types but especially prevalent in endothelial cells (93). Caveolae mediation relies on oligomerisation of the caveolins present in the membrane,

which will induce invagination and formation of the endocytic vesicle. These vesicles are ~50 – 60 nm in diameter, notably flask-like in shape, and are trafficked similarly to clathrin-mediated endocytic vesicles (94). The characteristic shape is conferred by caveolin; a diametric cholesterol binding protein. It has been found that opportunistic viruses such as SV40 are able to take advantage of this pathway as an entry route into the cell, and it was by studying this trafficking that the pathway was elucidated however the signalling cascades involved have yet to be well characterised (95). The size of the caveolae infers that there is little space for fluid phase uptake and that the process is highly regulated by its cargo. It is also a process triggered by specific receptor binding and is thus specific to its cargo, unlike clathrin-mediated endocytosis.

Macropinocytosis (Fig. 1.4 b) is a third method of internalisation which refers to the ruffling or invagination of the cell membrane in such a way that large quantities of external environment can be internalised in the vesicle in proportion to their concentration external to the cell. It is usually induced by receptor binding of growth factors triggering the necessary acting growth near the cell membrane enveloping the 'ruffle' (95). Macropinocytosis is a source of massive fluid phase internalisation and constitutes the largest source of uptake of soluble nutrients and peptides (95). The fate of macropinosomes depends on the cell type. In macrophages, they merge completely into a late endosome and later into the lysosomal population and share the same physiology of any other lysosome (96), however in human carcinoma cells, they are known to remain discrete and not

interact with the lysosomal population and are recycled back to the cell surface membrane (97). Though less common, macropinocytosis is clearly a key gateway for constitutive uptake which can be exploited for drug delivery given a high enough extracellular concentration.

All of these pathways may be exploited to gain access to the internal milieu of the cell (85). However, a robust understanding of the next steps taken in the journey of silk nanoparticles through the cell is important to be confident in the efficacy of both the drug carrier and the chosen route of delivery.

It is important to characterise the trafficking of silk nanoparticles through a cell in order to ensure correct drug delivery and to establish a basis for the intracellular fate of these nanoparticles and to provide further evidence that silk nanoparticles are stable contenders for intracellular drug delivery.

To investigate the intracellular fate of silk nanoparticles, various methods can be used including subcellular fractionation and fluorescence microscopy. It is common to use primarily a microscopy-based technique to achieve this as it is both a well-established method and procedurally less complex, but microscopy alone does not give us a full picture.

The advantage of subcellular fractionation lies in the fact that it is quantitative and extremely accurate if carried out correctly, providing an excellent opportunity for

us to explore the intracellular fate of silk nanoparticles. Figure 1.6 provides an overview of the place of subcellular fractionation in this process. Its power to quantitatively determine the presence of nanoparticles means that it has found a place at the core of this research; it allows us to exploit the EPR effect to direct a nanomedicine to a tumour or cell culture of interest in vitro (fig. 1.5 a), allow its uptake via endocytic pathways (fig. 1.5 b) and distribution via intracellular trafficking (fig. 1.5 c), and then quantitatively trace its fate within the cell (fig. 1.5 d). However subcellular fractionation is not without its flaws, as discussed below.

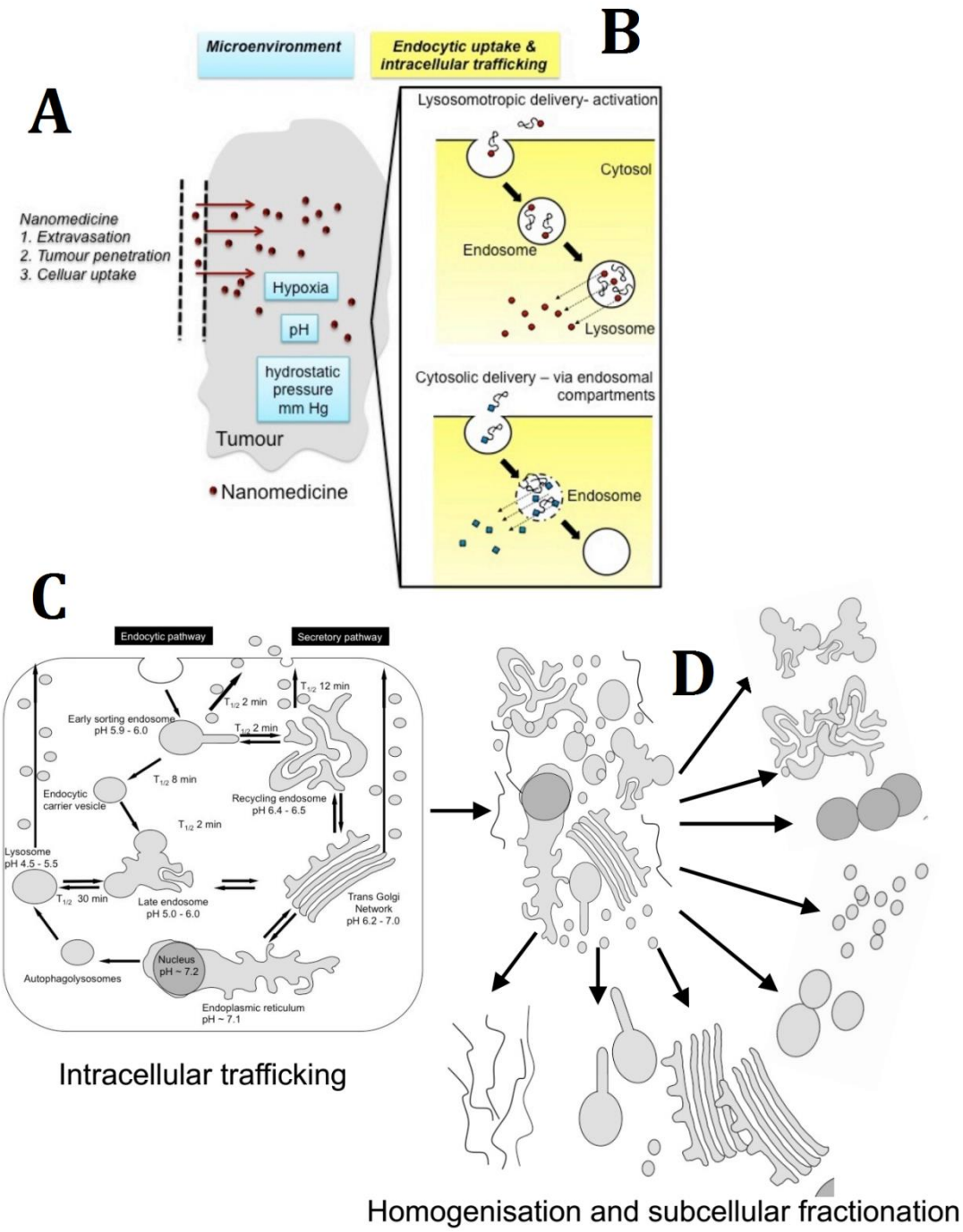

Figure 1.5 Overview of the place of subcellular fractionation in a scheme of work elucidating the intracellular fate of nanoparticles, showing delivery (a), uptake (b), trafficking (c), and finally homogenisation and fractionation (d)

1.5 An overview of fractionation

Meischer is credited with having first used centrifugation for the purposes of separating cellular organelles, when he separated the nuclei from human pus cells (98). Though crude and unrefined, the results of his work gave us a first glimpse into the inner structure of a cell.

From there, the methods and results have only become more refined, and as such fractionation by way of a centrifuge has played a pivotal role in exploring the cell, with Bensley using more refined methodologies to isolate and analyse pure mitochondria (99) and Claude using similar techniques to analyse microsomes (100). A pioneer of the field, de'Duve, refined these techniques even further and, with not inconsiderable effort, discovered, isolated and characterised lysosomes, winning the Nobel Prize alongside Claude and Palade in 1974.

Though already a powerful tool, it was really de'Duves' and Claude's work which refined fractionation to the point where it became an indispensable tool for microbiologists. Claude, in 1944 and 1945, published two papers wherein he detailed the first quantitative methodology for tissues fractionation (100,101) and de'Duve, in the 1950s used these methods to isolate the lysosome (9).

Later, Hodgeboom in collaboration with Schneider published a series of papers detailing the distribution of enzymes and their activities with respect to the

distribution of organelles in the fractionated samples (102), allowing the identification of fractions based on the activity of various marker enzymes.

As a direct result of this work, subcellular fractionation has become a refined and remarkably precise tool. The road to its refinement has been a long one, and at times difficult to traverse, as the technology has not always been present in order to validate the results, a prime example being the isolation of chromatin strands by Claude (103), but with the inability to properly survey the purity of the sample. In this respect, the limiting factor on fractionations growth has at times been the technology around it.

Subsequently, tissue fractionation has grown from an art to become the gold standard for quantitatively assessing the localisation of intracellular components, finding uses primarily in proteomics and drug trafficking.

1.6 The physical basis of subcellular fractionation

Subcellular fractionation relies upon the exploitation of the physical properties of small particles or organelles and how this determines their behaviour under high relative centrifugal force (RCF).

A centrifuge, at its most fundamental level works on the principal of centripetal acceleration whereby, if accelerated around a fixed axis, an object accelerated thusly will come under the influence of a force perpendicular to the plane of the axis, simulating increased gravity in that direction known as RCF.

Tissue fractionation exploits the hydrodynamic properties of particles under extremely high RCF. An understanding of the physical properties of a given particle is vital to being able to most effectively exploit these phenomena.

Any particle in a hydrodynamic system possesses a value known as its 'Stokes radius'. The Stokes radius is the radius of a hard sphere which diffuses at the same rate as that solute or particle in a given solvent as calculated by the Stokes equation (equation 1.).

$$F_{drag} = 6\pi\mu RV$$

F_{drag} = Frictional force acting on the sphere (N)
μ = Dynamic viscosity of the media through which the sphere is moving (Pa s)
R = Radius of the spherical object (m)
V =Flow velocity relative to the spherical object (m/s)

Equation 1. The Stokes equation.

Particles with a larger Stokes radius will typically sediment faster, being more massive and those with a smaller Stokes radius will sediment more slowly. As with any fluid system these particles will have, as a function of their Stokes radius, a terminal velocity through the medium. It is this difference in mobility we exploit.

Stokes' law makes a number of assumptions about the system in order to work. Firstly, it assumes a system wherein the solvent is of a constant viscosity, secondly it assumes laminar flow during sedimentation and finally it fails to take account of interference caused by particles in the system. However it does account for solute effects and can be adjusted accordingly, however that is not relevant here, when simply looking at macromolecules on a large scale.

By exploiting the differing Stokes radii and the implicit drag coefficient of different organelles, we can accurately fractionate a cellular homogenate by organelle size and density; and assay for marker enzymes associated with them in order to identify discrete fractions.

1.7 Current use of subcellular fractionation

Subcellular fractionation owes its popularity to its ability to isolate the components of a cell and allow us to identify, purify and interrogate them using methods such as: enzyme assays, radio- or fluoro- tagging of particular components; or even fluorescence microscopy of a fraction. This ability however, presents its own set of problems.

The controls required for such identification require careful optimisation with consideration for the amount of cellular material available for use in these assays.

Subcellular fractionation is used to trace the intracellular fate of nanoparticle trafficking. It has been used to elucidate the fate and test the toxicity of zinc oxide nanoparticles in earthworms as a model for the potential biological effects and environmental outcome (57). It has also been used recently to trace the fate of cobalamin, or vitamin B12 in human neurons and fibroblasts, investigating the role of lysosomes in possible age-related pathological processes (104). The trafficking of trivalent metal ions such as aluminium (Al^{3+}) and scandium (Sc^{3+}) in algae has also been elucidated using subcellular fractionation, examining the suitability for the replacement of Al^{3+} by Sc^{3+} in uptake studies due to scandium's radioactive isotope Sc-46 (105).

Subcellular fractionation has also been a vital tool in the isolation of a particular cellular organelle. It is routinely used to isolate organelles for further interrogation

(106–108). However, it is rarely used in the context of tracing nanoparticles through a cell with the majority of the literature using microscopy-based techniques which while qualitative do not offer the whole picture. Subcellular fractionation bridges this gap and allows us to trace nanoparticles quantitatively, and is thus an important tool to be used in tracing silk nanoparticles.

1.8 Fractionation as a practical technique

Subcellular fractionation requires a number of finely optimised preparative steps before the actual fractionation and interrogation of those fractions can take place. The primary focus of this thesis is laying the groundwork for the development of these methods. The first of these is the preparation of a cellular homogenate.

It is important to note that fractionation is not without its share of weaknesses. As with any method there are drawbacks associated with drawing a high level of accuracy from what is a comparatively gross preparation of cellular homogenate.

The first is the need for the use of marker enzymes to identify fractions based on organelle content. Due to the nature of the procedure, these marker enzymes will exhibit a distribution over all fractions; merely highlighting the fraction where their activity is comparatively high.

This requirement places a restriction on the amount of material available for each assay, and then on the amount of material from each fraction available for interrogation. For example, a fractionation scheme requiring the identification of the nuclear, mitochondrial, lysosomal, cytosolic, and plasma membrane fractions will require five samples for fraction identification and then a sixth, larger sample for interrogation.

Furthermore, it is a particularly gross method. We are unable to have a fraction of the mitochondrial components of the homogenate either pure or in its entirety, as it will be dispersed along the entire homogenate, and will contain in very small amounts, components from other cellular compartments. Due to this we cannot consider our fractions to be pure per se, but instead must view them as a snapshot across the more highly concentrated abundance of our target organelle. Similarly, there is a need to account for all observed enzyme activity in an unfractionated in order to determine total activity against which the activity in individual fractions by be compared.

Fractionation is very labour intensive, given the number of control experiments required, the optimisation and the interpretation of results factoring in all required controls. Being a particularly gross method, it is important to be as precise as possible when interpreting any data gathered.

As previously stated, fractionation requires assays to be run in order to identify fractions since they have been produced. These assays must be chosen very carefully, to ensure the activity is unique to the organelle we are attempting to identify. Additionally, it must be ensured that the resulting products for the reaction are stable, and again unique to the reaction specifically, in order to ensure that the data we acquire is representative of the fraction we are observing, and not fettered by the presence or activity of other enzymes with similar activity with the same substrate. For this reason, markers are chosen which have no cross-reaction

or whose reactions render similar products, and which are suitably sensitive enough for the quantities of product expected in our homogenate.

The marker enzymes chosen for this study were based on work previously undertaken by Seib et al (8) as the work undertaken there closely mirrors the aims of this study. However before establishing the marker assays in the lab, it was imperative to ensure that each assay had been selected in order to prevent any crossover between the substrates used for the enzyme assays. The selected marker assays are summarised in table 1.3, along with their substrates, measured compounds and original sources for their development or adaptation.

The nature of the preparation of the cellular homogenate is such that it is impossible to attain a homogenate of consistent cellular concentration due to slight variances in procedures due to human or equipment error. Because of this, simply measuring the enzyme activity (mol/min) present in the sample is grossly inaccurate, considering the size of the samples used and the low concentrations of product expected. In order to normalise enzyme activity, it is necessary to compare the enzyme activity to the concentration of the cellular homogenate, which can be accurately determined by protein concentration. The measurement of enzyme activity normalised to protein content is specific enzyme activity, which is expressed as (mol/min/mg). This was also applied to the DAPI assay, normalising fluorescence and DNA content against protein concentration.

Table 1.3 The markers chosen to identify individual fractions and the compounds used to identify their presence.

Fraction	Marker	Compound identified	Type of assay	Reference
Cell surface membrane	Alkaline phosphatase	4-nitrophenol	colourimetric	(49)
Mitochondrial	Succinate dehydrogenase	Iodonitrotetrazolium violet-formazan (INT)	colourimetric	(49)
Cytosolic	Lactate dehydrogenase	Pyruvate	colourimetric	(109)
Lysosomal	N-acetyl-ß-glucosaminidase	4-Methylumbelliferone	colourimetric	(110)
Nuclear	DNA	DNA-bound DAPI	Fluorescent	(49)

Protein concentration was determined using a bicinchoninic (BCA) assay, which takes advantage of the development of an intense purple colour developing following the reaction between Cu^{+} and BCA following the conversion of Cu^{2+} to Cu^{+} induced by reaction of Cu^{2+} with peptide bonds (111).

The protein content of the homogenate is expressed as mg of protein per ml of cellular homogenate (mg/ml).

Finally, when tracing the fate of nanoparticles, it is entirely possible for the particles whose fate we are tracing to affect the natural buoyancy and thus Stokes radius of the organelles examined and this must be taken into account when choosing for example, the fractionation media.

As mentioned previously, subcellular fractionation has been used in tracing intracellular fates of components extensively, but is often accompanied by a number of other methods in order to corroborate the findings. Primarily fluorescence microscopy is used for this purpose, being especially good at highlighting large abundances of fluoro-tagged molecules. This ability makes it very easy to, on a qualitative level, identify their localisation and narrow a search for fractionation, or to highlight any potentially erroneous data.

2 Aims

There was a need to establish a number of biochemical assays in the laboratory in order to underpin future studies aimed at tracing the intracellular fate of silk nanoparticles in B16F10 cells. Therefore, this thesis aims to establish wet lab validated marker assays for intracellular organelles. The specific aims were:

1. Establish the efficient homogenization of B16F10 cells.
2. Establish we lab validated marker assays for; mitochondria, lysosomes, plasma membrane, cytosol and the nucleus.
3. Perform a preliminary study of silk nanoparticle's cytotoxicity in B16F10 cells

3 Materials and methods

3.1 Table of materials used

Material	Purity	Catalouge number	Supplier	Supplier location
2-[4-(2-hydroxyethyl)piperazin-1-yl]ethanesulfonic acid (HEPES)	≥99.5%	H3784-25g	Sigma Aldrich	Dorset, UK
2-p-iodo-phenyl-3-p-nitrophenyl tetrazolium chloride	95%	I10406	Sigma Aldrich	Dorset, UK
3-(4,5-Dimethylthiazol-2-yl)-2,5-Diphenyltetrazolium Bromide (MTT)		M6495	Fisher Scientific	Carlsbad, California, US
4',6-diamidino-2-phenylindole	>90%	1023.627.6001	Roche Diagnostics via Sigma Aldrich	Dorset, UK
4-methylumbelliferyl N-acetyl-β-D-glucosaminidase		M2133-25Mg	Sigma Aldrich	Dorset, UK
Aprotinin from bovine lung		10236624001	Roche Diagnostics via Sigma Aldrich	Dorset, UK
Boric Acid	≥99.5%	B6768-500g	Sigma Aldrich	Dorset, UK
B16 F10 Musc musculus melanoma cells		CRL-6475	American Type Culture Collection (ATCC)	
Dextran 15,000-25,000 g/mol		31387-100g	Sigma Aldrich	Dorset, UK
Dimethylsulfoxide (non sterile)	≥99.9%	D8418	Sigma Aldrich	Dorset, UK
Ethyl acetate	99.80%	270989 1l	Sigma Aldrich	Dorset, UK
Ethanol	≥99.8%	32221	Sigma Aldrich	Dorset, UK
Fetal Bovine Serum		10500-064	Gibco	Carlsbad, California, US

Glycine	≥99%	G7126-500g	Sigma Aldrich	Dorset, UK
Hydrochloric acid solution (HCl) 1 M		71763-1L	Sigma Aldrich	Dorset, UK
Leupeptin	≥90%	L2884	Sigma Aldrich	Dorset, UK
Lithium Bromide	≥99%	746479-500G-D	Sigma Aldrich	Dorset, UK
Magnesium chloride	≥98%	M8266-100g	Sigma Aldrich	Dorset, UK
Micro bicinchoninic acid (BCA) assay kit		23235	Fisher Scientific	Carlsbad, California, US
Polyethylenimine, linear (PEI) average 10,000 g/mol		765090-1g	Sigma Aldrich	Dorset, UK
Penicillin G sodium salt		P3032-25MU	Sigma Aldrich	Dorset, UK
Pepstatin	≥90%	P5318	Sigma Aldrich	Dorset, UK
Phenylmethanesulfonylfluoride (PMSF)		PMSF-RO ROCHE	Sigma Aldrich	Dorset, UK
p-nitrophenol phosphate	≥99%	71768-5g	Sigma Aldrich	Dorset, UK
Pyruvate	≥99%	P5280-25g	Sigma Aldrich	Dorset, UK
RPMI 1640		R8758-24X500ML	Sigma Aldrich/Gibco	Dorset, UK
Sodium bicarbonate	≥99%	S8875-2.5KG-D	Sigma Aldrich	Dorset, UK
Sodium chloride (NaCl)	≥99.8%	S3014-500g	Sigma Aldrich	Dorset, UK
Sodium hydroxide (NaOH)	≥98%	S8045-500g	Sigma Aldrich	Dorset, UK
Sodium succinate	≥99%	S5047	Sigma Aldrich	Dorset, UK
Streptomycin sulfate salt		S9137-25G	Sigma Aldrich	Dorset, UK
Sucrose	≥99.5%	S9378-500g	Sigma Aldrich	Dorset, UK
Trisbase	≥99.9%	T1503-25g	Sigma Aldrich	Dorset, UK
Trichloroacetic acid	≥99%	T6399 100g	Sigma Aldrich	Dorset, UK
Tris-HCl	≥99%	T3253-250g	Sigma Aldrich	Dorset, UK
Trypan blue 0.4%		T8154-20ML	Sigma Aldrich	Dorset, UK
Trypsin-ethylenediaminetetraacetic acid (EDTA)		25200-056	Gibco	Carlsbad, California, US

3.2 Cell Culture

The cells chosen for experimentation were B16F10 (ATCC CRL-6475) mouse melanoma cells.

Cells were cultured in RPMI 1640 (Sigma Aldrich/Gibco) medium supplemented with 10 v/v % FBS (Gibco 10500-064) and 1 % v/v penicillin – streptomycin solution in cell culture treated flasks (Corning T72 and T175) to allow cell adhesion.

In order to harvest cells, the medium was aspirated with a Pasteur pipette. The cells were washed twice with 10 ml phosphate buffered saline (PBS) at room temperature. Next, the cells were incubated with 2 ml of 0.25 v/v % trypsin ethylenediaminetetraacetic acid (EDTA) (Gibco 25200-056) for five minutes at 37 ˚C and 5 % CO_2. Next, 8 ml of complete culture medium was added to the flask to inhibit trypsin activity. The suspension was removed and centrifuged for 4 minutes at 380 x g (1500 RPM) in a Hettich Rotofix 32A centrifuge with a 1619 swing bucket rotor.

The supernatant was aspirated, the pellet agitated and the cells resuspended in 10 ml complete culture medium. The cell suspension was typically split at a ratio of 1:10 suspension to media into a new growth flask and left to incubate at 37 ˚C and 5 % CO_2.

3.3 Cell harvesting for homogenisation

Cells harvested for homogenisation were grown as above in a T175 cell culture treated flask and then split in a 1:10 ratio into 15 separate 150 mm cell culture treated Petri dishes. These were incubated for 72 hours at 37 °C. Following incubation, the medium was aspirated and the plates were washed twice with 15 ml PBS at 4 °C. 15 ml PBS at 4 °C was added to the plate and a cell scraper used to detach cells from the plate. The resulting suspension was transferred to a 50 ml Falcon tube at 4 °C. A further 15 ml of PBS at 4 °C was added to the plate, the plate turned through 90 ° and the scraping repeated. Once all plates had been harvested, the suspension was centrifuged for 4 min at 380 G (1500 RPM) in a Hettich Rotofix 32A centrifuge with a 1619 swing bucket rotor. The resulting pellets were combined and resuspended in 2.5 times the pellet weight of homogenisation buffer.

3.4 Homogenisation buffer

20 µl of 1mg/ml aprotinnin, 20 µl of 1 mg/ml leupeptin (Sigma Aldrich L2884), 10 µl of 1 mg/ml pepstatin (Sigma Aldrich P5318) and 100µl of 17mg/ml phenylmethanesulphonylfluoride (PMSF) (Sigma Aldrich PMSF-RO ROCHE) were added to 250 mM sucrose containing 1 mM EDTA and 10 mM 2-[4-(2-hydroxyethyl)piperazin-1-yl]ethanesulphonic acid (HEPES) (Sigma Aldrich –

H3784-25g). PSMF was made freshly every instance and protease inhibitors were frozen and added separately.

3.5 Homogenisation

Fractionation was carried out using a cell cracker as previously described in Gruenberg and Howell (1968) (Figure 3.4.1). A ball bearing of clearance 7 µm was used. Prior to homogenisation, the cell cracker was primed with homogenisation buffer, using a 1ml syringe. The first pass was run through from the opposite side from which the priming was performed. Following each pass, 60 µl of sample was taken to perform an *N*-acetyl-ß-glucoseaminidase assay to determine latent activity of the lysosomal enzyme as an indicator for organelle breakage, and 10 µl to perform the lactate dehydrogenase assay to determine cell homogenisation efficiency.

Figure 3.4.1: A cell cracker displaying inner race and ball bearing assembly.

3.6 MTT (3-(4,5-Dimethylthiazol-2-yl)-2,5-Diphenyltetrazolium Bromide) assay for cell growth.

Growth curves were run for B16F10 cells at cell densities of 500 and 5000 cells/cm^2.

Cells were harvested as detailed above and a 100 µl sample was added to 100 µl trypan blue (Sigma Aldrich T8154-20ML). A haemocytometer was used in conjunction with a phase contrast microscope to determine cell concentration in the suspension.

They were then diluted in 12 ml of complete media and seeded with 100 µl cell suspension in a cell culture treated 96-well plate well.

The cells were allowed to recover for 24 hours. Once every 24 hours for the following 5 days, 20µl of 3-(4,5-Dimethylthiazol-2-yl)-2,5-Diphenyltetrazolium Bromide (MTT) (Fisher Scientific M6495) at 5 mg/ml in PBS was added and allowed to incubate for 5 h. Following incubation, the wells were aspirated carefully, and 110 µl of dimethylsulphoxide (DMSO) (Sigma Aldrich D8418) added to each well and incubated for a further 5 min to allow dissolution of the formazan crystals.

Finally, 100 µl of the DMSO/formazan was transferred to a fresh 96 well plate and the absorbance read at a wavelength of 570 nm. All DMSO was removed and replaced with 100 µl of PBS.

All wells on the outside of the plate were not used in any measurements, to avoid any anomalies due to media evaporation.

3.7 Cytotoxicity assays

Positive and negative control

To measure cell viability over a range of concentrations of polymers, an MTT assay was used as above with the following modifications. A cell density of 5000 cells/cm^2 was used. Wells contained polyethylenimine (PEI) (Sigma Aldrich - 765090-1g) or dextran (Sigma Aldrich - 31387-100g) for the positive and negative controls respectively, dissolved in complete media over a concentration range of 0 to 200 μg/ml. Media was added first to the well before a quantity of the stock dilution of PEI or Dextran.

The cells were then incubated for 72 hours at 37 °C and 5 % CO_2. Following incubation, an MTT assay was performed as above. Each control was run in triplicate.

3.8 Determination of alkaline phosphatase activity (Plasma membrane)

200 μl of 25 mM boric acid (Sigma Aldrich – B6768-500G) / 8 mM *p*-nitrophenol phosphate (Sigma Aldrich, 71768) / 2 mM $MgCl_2$ (Sigma Aldrich – M8266-100g) solution was added to 50 μl of homogenate in a 1.5 ml microcentrifuge tube. This

was incubated at 37 °C for 1 h. The reaction was quenched by the addition of 600 µl of 250 mM NaOH (Sigma Aldrich – S8045-500g).

The mixture was centrifuged for 20 min at 700 x g and 200 µl of supernatant was added to the well of a 96-well plate and absorbance measured at a wavelength of 405 nm. 200 µl of 25 mM boric acid / 8 mM *p*-nitrophenol phosphate / 2 mM $MgCl_2$ solution was used as a blank.

Activity was calculated using a standard curve of *p*-nitrophenol phosphate.

3.9 Determination of Succinate Dehydrogenase activity (Mitochondria)

250 µl of 20 mM Tris-HCl (Sigma Aldrich T3253 250g)

(pH 7.4) 0.1 mM EDTA, 50 µl of 200 mM sodium succinate (pH 7.5) (Sigma Aldrich S5047) and 50 µl of 2.5 mg/ml was added to a 2 ml microcentrifuge tube. 50 µl of homogenate was added to start the reaction and the mixture was incubated at 20-23°C for 10 min. The reaction was stopped with the addition of 1 ml of a 5:5:1 ethyl acetate (Sigma Aldrich 270989 1l) / ethanol (Sigma Aldrich 32221) / trichloroacetic acid (Sigma Aldrich T6399 100g). The mixture was centrifuged at maximum speed in a bench top centrifuge for 2 min, the supernatant removed and absorbance read at a wavelength of 500 nm.

3.10 Quantification of DNA (Nucleus)

To 33 µl of 4',6-diamidino-2-phenylindole (DAPI) (Roche Diagnostics 1023.627.6001 10 mg) was added to 17 µl of sample in a 2 ml Eppendorf tube and made up to 2 ml with 1950 µl of 12 mM NaCl (Sigma Aldrich – S3014-500g), 5 mM HEPES (pH 7). 200 µl of the resulting solution was added to a black 96-well plate (Sigma Aldrich M0312-32EA), and measured at an excitation wavelength of 372 nm and an emission wavelength of 454 nm. Quantities were determined by comparison against a standard curve. All steps were carried out using low DNA binding tips and tubes.

3.11 Determination of lactate dehydrogenase activity (Cytosol)

250 µl of 81.3 mM Tris (Sigma Aldrich - T1503-25), 203.3 mM NaCl, 0.244 mM NADH (Sigma Aldrich – N8129-50mg) (pH 7.2) was added to the wells of a clear 96-well pate. 5 µl of sample was added to the wells and left to incubate at 30 °C for 2 min. 50 µl of Tris 81.3 mM, NaCl 203.3 mM, 9.76 mM pyruvate (Sigma Aldrich – P5280-25g) was added and its optical density (OD) measured immediately at 339 nm, and every 10 seconds thereafter for 20 minutes.

For a blank, the above method was used with 5 µl of homogenisation buffer in place of the 5 µl of sample.

3.12 Determination of N-acetyl-ß-glucosaminidase activity (Lysosomes)

100 µl of sample was added to 100 µl of 1 % Triton X-100 in homogenisation buffer, and left to incubate for 3 min. 50 µl of the Triton/sample mixture was added to 30 µl of 5 mM 4-methylumbelliferyl N-acetyl-β-D-glucosaminidase (Sigma Aldrich - M2133-25MG) 250 mM sucrose (Sigma Aldrich – S9378-500g) / 200 mM sodium citrate – HCl buffer (pH 5.0) and left to incubate for exactly 1 min in the dark at 25 °C. The reaction was stopped with the addition of 200 µl of 250 mM Glycine (Sigma Aldrich - G7126-500) /NaOH at pH 10.4. The microcentrifuge tube was then centrifuged at maximum speed in a bench top centrifuge for 2 min. 200 µl of the supernatant was removed and placed in the well of a black 96-well plate and read at an excitation wavelength of 360 nm and an emission wavelength of 448 nm.

3.13 Determination of the protein content of a sample

Quantification of the protein concentration of sample was conducted using a micro bicinchoninic acid (BCA) assay kit (Thermo Fisher Scientific - 23235). Once the working reagent had been mixed, 200 µl were added to a 96-well plate with 50 µl of sample and left to incubate at 37 °C for 30 min. Because this is not an end point assay, every sample was accompanied by a standard curve run in triplicate using bovine serum albumin as a standard from 1 mg/ml to 10 µg/ml. Absorbance was read at 562 nm.

3.14 Silk nanoparticle production

Silk cocoons from the silkworm *B. mori* (supplied by Tajima Shoji, Japan) were emptied, cut and boiled in 2 l of sodium bicarbonate (Sigma Aldrich S8875-2.5KG-D). The resulting fibroin was washed three times in 1 l distilled water for 20 min each and then dried and dissolved in 4 ml of 9.3 M LiBr (Sigma Aldrich 746479-500G-D) to every 1 g of fibroin. This was then dialysed against distilled water for 72 h, changing the water at discrete intervals.

The proportion of silk in solution was assessed by weighing 1ml of the solution and allowing it to dry overnight at a low heat in an oven. The sample was then weighed a second time. This gave a weight to weight proportion of silk to water. The resulting aqueous solution was then added drop wise to acetone keeping a ratio of >75% acetone to silk solution. The nanoparticles were then centrifuged at 48,000 x g for 2 h, washed in distilled water, sonicated twice at 30 % amplitude for 30 s and resuspended, repeated at least three times.

The resulting particles were resuspended in 10 ml distilled water and pooled. They were then centrifuged at 48,000 RCF for 2 h and resuspended in 5 ml distilled water to produce a highly concentrated solution.

3.15 Silk nanoparticle cytotoxicity assay

Silk nanoparticles in suspension at 22.93 mg/ml were gamma sterilised at 20 gray (Gy). A sterile stock solution was made up in distilled water to 1 mg/ml and 100 µg/ml, and made up into media at concentrations of 200, 180, 140, 100, 20, 10, 5,

2, 1 and 0 μg/ml. Care was taken to add the media before the silk nanoparticle stock in order to minimise any shock to the cells at a high concentration.

Following incubation for 72 h at 37 °C and 5 % CO_2, an MTT assay was performed as above.

3.16 Silk nanoparticle characterisation

Silk nanoparticles (SNPs) were characterised using a Malvern Zetasizer to determine size, polydispersity, zeta potential and mobility. A suspension of SNPs at 200 μg/ml was used in all cases.

3.17 Statistical analysis

All data was recorded and managed using Microsoft excel, and all graphs drawn and annotated using Graph pad Prism 4. Standard error of the mean (SEM) was represented using error bars and the number of replicates run denoted by n. Results were interpreted using Mintitab V17.3.1. Significance of results was determined using ANOVA, where statistical significance was assigned to $p < 0.05$.

4 Results

Standard curves were produced according to the assays used, with care to cover the required range. The assays were applied to homogenates produced in the same manner and standard curves used to determine enzyme specific activity, DNA concentration and protein concentration.

4.1 Marker assays

4.1.1 Assay Calibration curves

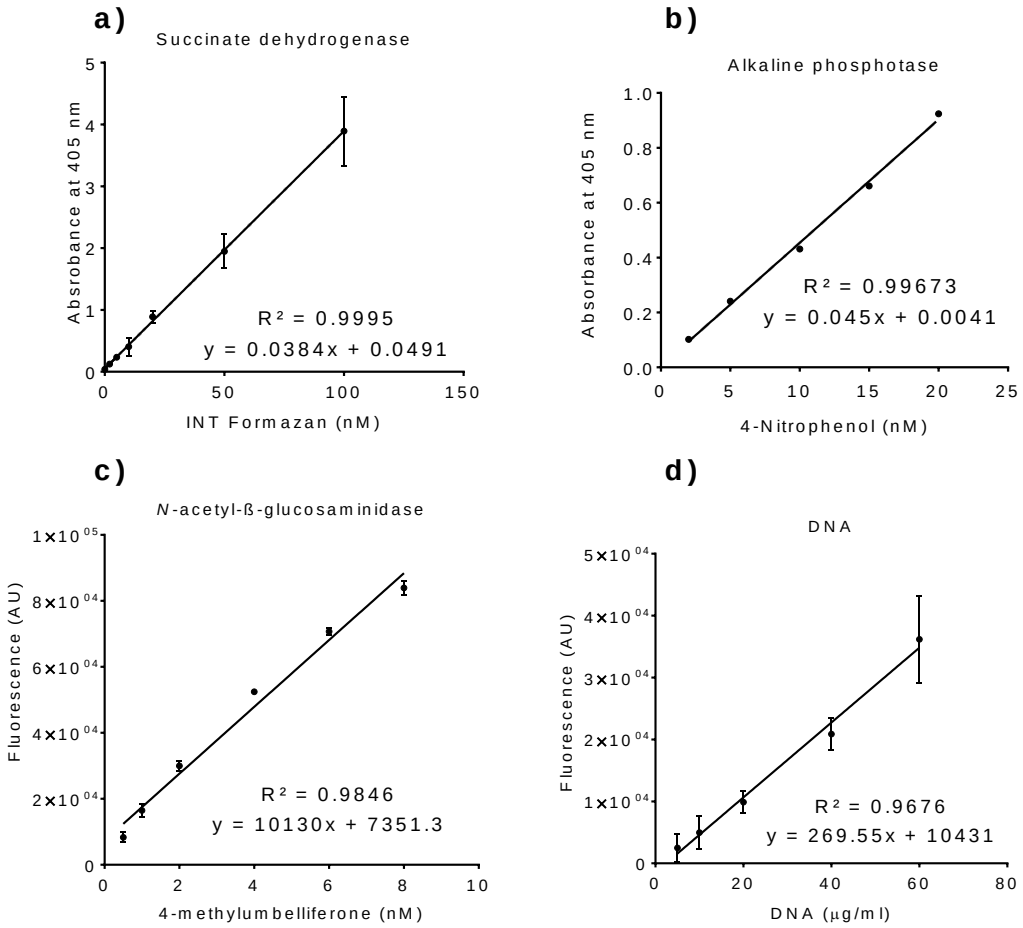

Fig 4.1 Calibration curves for (a) SDH and (b) ALP colorimetric assays and (c) N-acetyl-ß-glucosaminidase and (d) DAPI fluorescence assays. Error bars represent standard deviation and are inside plot symbols when not visible. n=3

The succinate dehydrogenase SDH calibration curve (a) showed linearity between absorbance at 405nm and INT-formazan concentration with an R^2 value of 0.999 between the INT-formazan concentrations of 2 and 100 nM.

The 4-nitrophenol standard curve (b) for the ALP assay showed a linear relationship between absorbance and 4-nitrophenol at concentrations between 2 and 10 nM with an R^2 value of 0.996 and low standard deviation across all data points.

The 4-methylumbilliferrone calibration curve (c) also shows linearity between concentrations of 0.5 and 8 nM with a R^2 value of 0.984.

The DAPI calibration curve (d) showed low standard deviation up to a DNA concentration of 60 µg/ml, beyond which point standard deviation increases. The R^2 value of 0.991 shows a linear relationship between DNA concentration and fluorescence at 454 nm.

4.1.2 Determination of protein concentration of homogenate

Protein concentration was determined using a Thermo Fisher micro BCA assay as described in the methods section. When determining protein concentration each assay was run alongside a calibration curve and values determined by absorbance at 562 nm. Fig 4.2 shows the protein concentration of each homogenate sample.

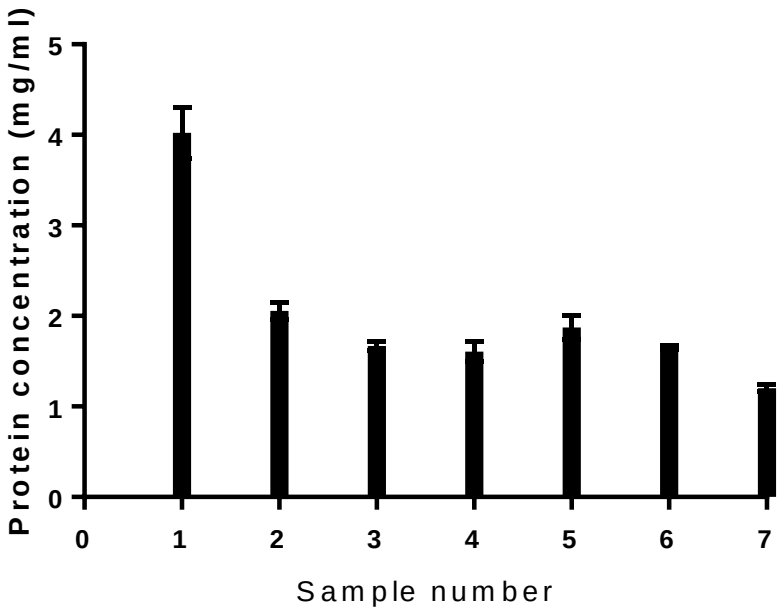

Fig 4.2 Protein concentration of cellular homogenate as determined by a BCA assay (n=3). Error bars represent standard deviation.

Protein concentration is consistent across homogenates following homogenisation and further dilution as stated in the materials and methods section. The samples were produced and stored during independent experiments. Sample one shows an unusually high protein concentration, due to omission of the final dilution step following homogenisation, as this was not considered necessary at the time.

The mean value for all homogenates is 2.01 mg/ml with a standard deviation of 0.92.

However, all following homogenates, which were prepared using a second dilution step, have a mean value of 1.6 and a standard deviation of 0.28.

4.1.3 Determination of ALP specific activity of homogenates

Alkaline phosphatase (ALP) activity was determined by way of the colourimetric assay outlined in the materials and methods section. The assay was applied to all homogenates at separate times following their homogenisation and the results applied to the standard curve. Fig 4.3 shows the ALP specific activity of each homogenate sample.

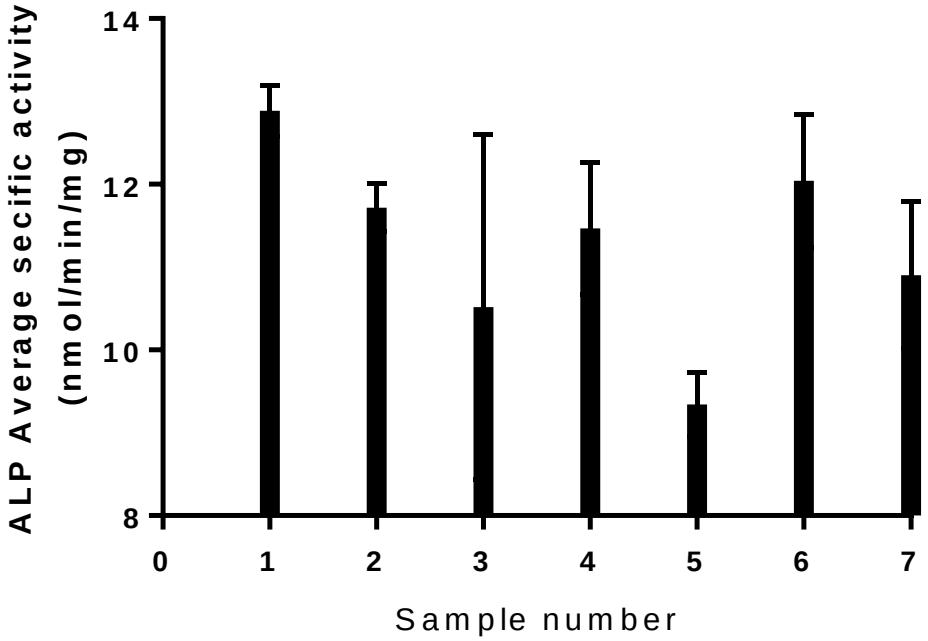

Fig 4.3: Specific activity of alkaline Phosphatase for all cellular homogenates (n=3). Error bars represent standard deviation.

ALP specific activity is consistent across, with the exception of the fifth sample and all homogenates shows a low standard deviation of 1.14 with an average specific activity of 11.2 nmol/min/mg.

4.1.4 Determination of SDH specific activity of homogenates

The specific activity of SDH was determined using a colourimetric assay, as outlined in materials and methods. Fig 4.4 shows the SDH specific activity of each homogenate sample.

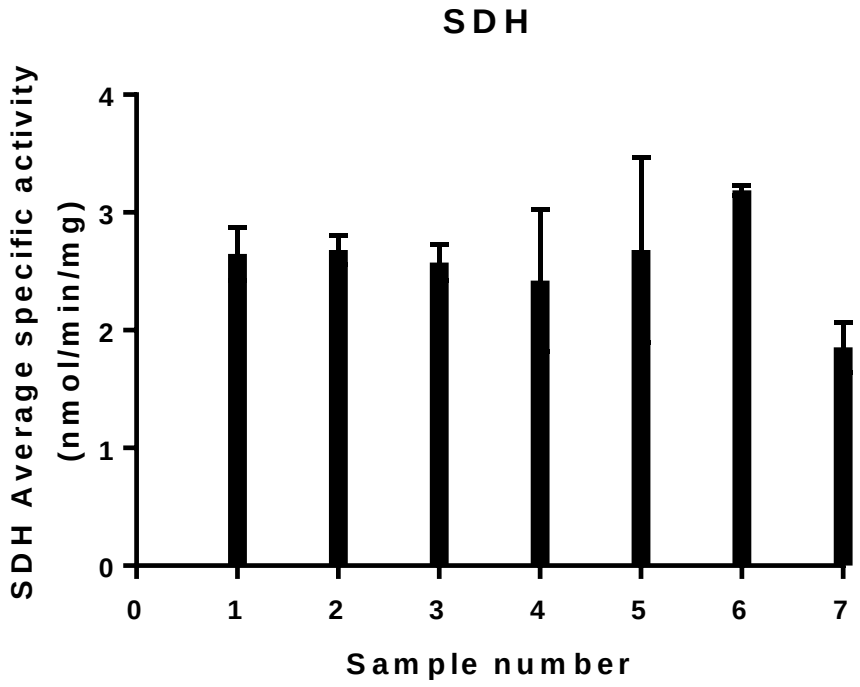

Fig 4.4 Specific activity of succinate dehydrogenase for all cellular homogenates (n=3). Error bars represent standard deviation.

SDH activity is consistent across homogenates, with an average specific activity of 2.3 nmol/min/mg and a standard deviation of 0.44. The standard deviation shows low variation across homogenates. However, there is a substantial drop from the mean specific activity for sample seven, which is discussed later.

4.1.5 Determination of DNA concentration of homogenates

DNA concentration was determined using a fluorescent DAPI assay as stated in the materials and methods. Fig 4.5 shows the DNA concentration of each homogenate sample.

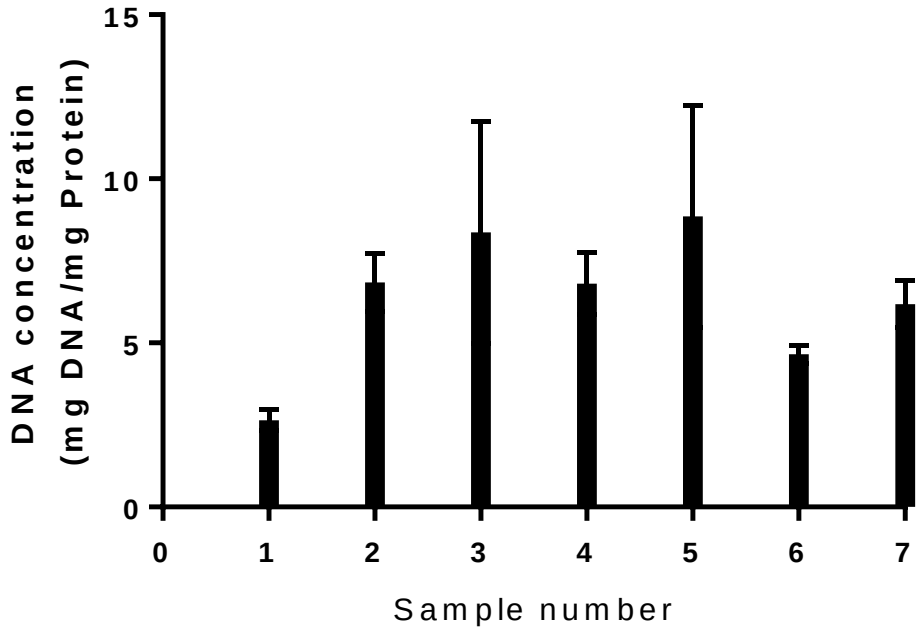

Fig 4.5 Concentration of DNA for all cellular homogenates (n=3). Error bars represent standard deviation.

DNA concentration varies between homogenates, with an average DNA concentration of 6.3 µg/ml and a standard deviation of 2.1 µg/ml. The high variation shows a low consistency across homogenates; however the possible reasons for this are discussed later. Measurements for samples one and six are substantially below the mean value, with all other readings being within a similar range.

4.1.6 Determination of LDH specific activity of homogenates

The activity of LDH in a sample was determined as stated in the materials and methods. Specific activity was determined using the published extinction coefficient of the coenzyme NADH in solution in distilled water (Dawson RB 1985). Fig 4.6 shows the LDH specific activity of each homogenate sample.

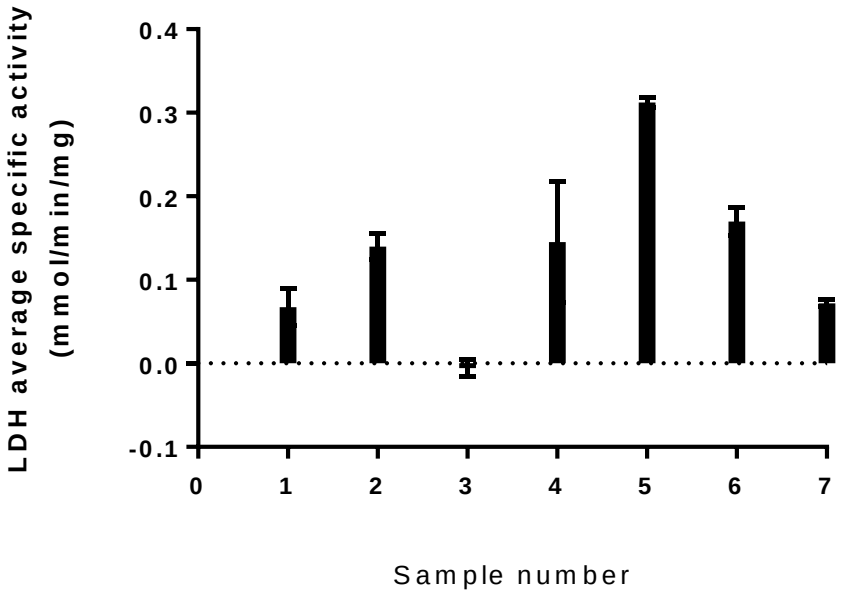

Fig 4.6 Specific activity of lactate dehydrogenase for all cellular homogenates (n=3). Error bars represent standard deviation.

Specific activity varies widely across homogenates, with sample three showing negative activity according to calculations, and samples one and seven showing low activity. The possible reasons for this are explored in the discussion. The average specific activity is 0.12 mmol/min/mg with a standard deviation of 0.1.

4.1.7 Determination of N-acetyl-ß-glucosaminidase activity of homogenates

N-acetyl-ß-glucosaminidase activity was determined using the fluorescence assay as outline in materials and methods. Fig 4.7 shows the N-acetyl-ß-glucosaminidase specific activity of each homogenate sample.

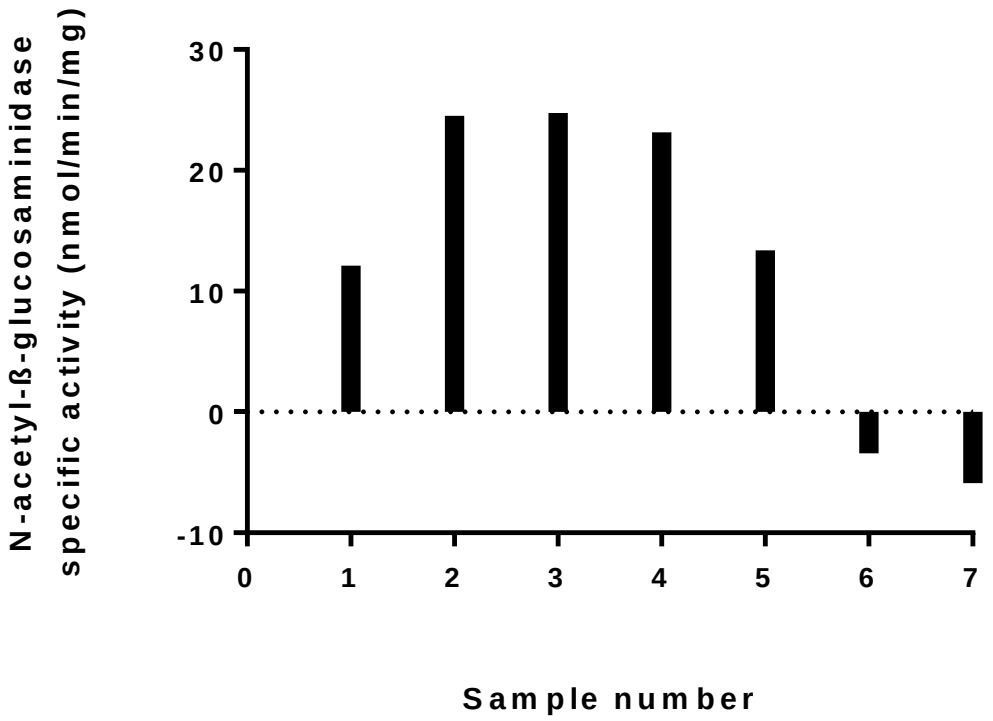

Fig 4.7 Specific activity of N-acetyl-ß-glucosaminidase for all cellular homogenates (n=1).

N-acetyl-ß-glucosaminidase activity varies significantly across homogenates, with samples six and seven showing negative activity. However, for a number of homogenates, readings appear to be consistent, namely two, three and four, the standard deviation is high at 12.9 considering the specific activity at 12.66 nmol/mg/ml, due in part to the readings taken on homogenates from samples six and seven. However, if samples six and even are omitted, the standard deviation drops to 10.85.

4.2 Growth curve of B16F10 mouse melanoma cells

Mouse melanoma cells B16F10 were cultured in 96 well plates as discussed in the materials and methods section, at a cell seeding density of 500 cells/cm^2 and 5000 cells/cm^2. The density of the resulting cell population was then assessed using an MTT assay. Fig 4.8 shows the recorded growth curves for B16F10 cells.

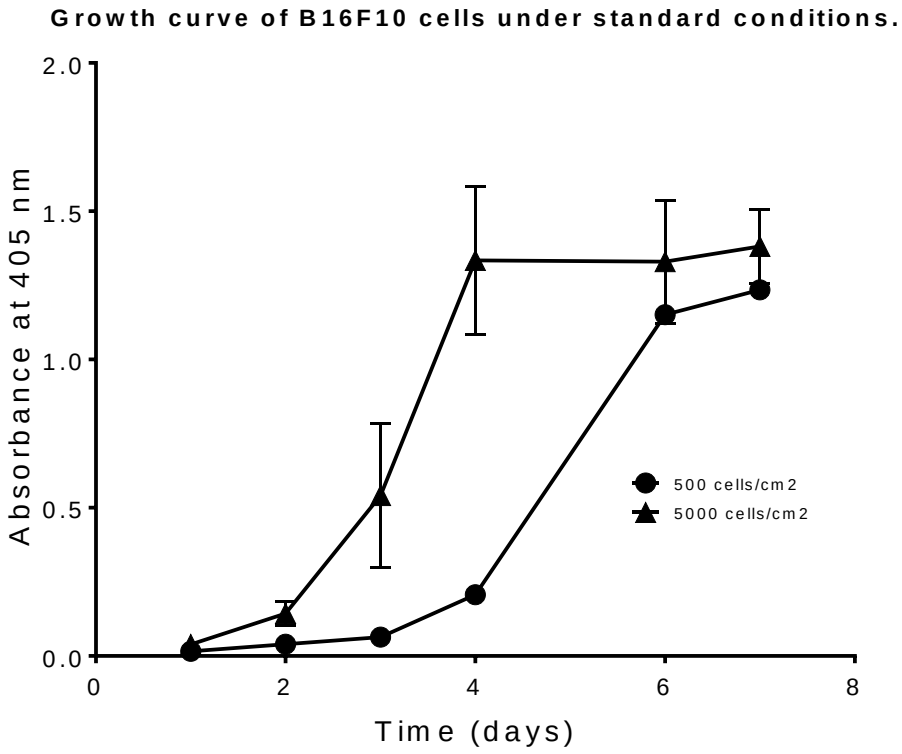

Fig 4.8. Growth curve for B16F10 cells seeded in densities of 500 and 5000 cells/cm^2 (n=3). Error bars represent standard deviation.

Cells seeded at 500 cells/cm^2 and 5000 cells/cm^2 show a lag phase lasting one day for 5000 cells/cm^2 and four days for cells seeded at 500 cells/cm^2. Exponential growth occurs between 2 and 4 days for cells seeded at 5000 cells/cm^2, and 4 and 6 days for cells seeded at 500 cells/cm^2. A plateau occurs as the culture reaches 100 % confluence at 4 days for cells at 5000 cells/cm^2 and at 6 days for cells seeded at

500 cells/cm^2. When initially cultured at a lower density the lag phase lasts almost twice as long before exponential growth is observed.

4.3 Cytotoxicity of SNPs

Cytotoxicity was determined by way of an MTT assay conducted on cells seeded at 5000 cells/cm^2 with dextran or PEI dissolved in the media as stated in the materials and methods section.

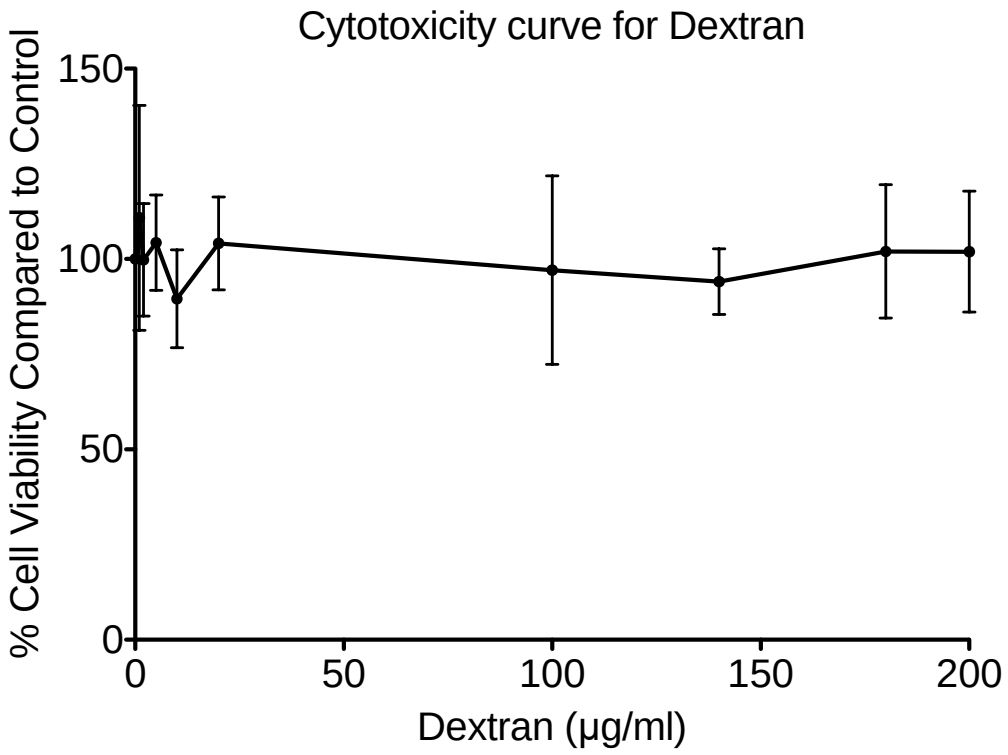

Fig 4.9 Cytotoxicity curve for dextran applied to B16F10 cells in concentrations from 1 to 200 µg/ml. (n=3). Error bars represent standard deviation.

Dextran shows low cytotoxicity with a minimum cell viability of 95.5% at a dextran concentration of 20 µg/ml however the standard error on these values is high. The IC50 of dextran is beyond the scale of the assay and as such is not determined here.

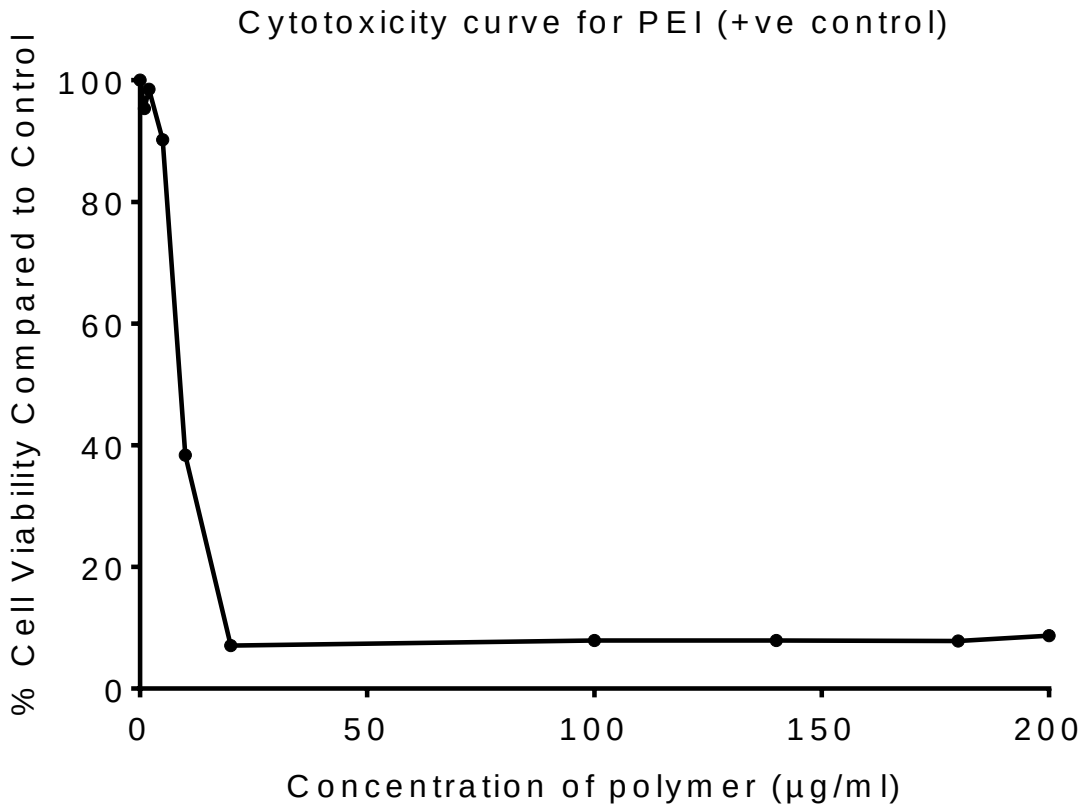

Fig 4.10 Cytotoxicity curve for PEI applied to B16F10 cells in concentrations from 1 to 200 µg/ml. (n=3)

Cytotoxicity of PEI as measured with an MTT assay. Error bars represent standard deviation and are within plot symbols when not seen.

PEI cytotoxicity is high in all but the lowest concentrations showing an IC50 of 8.8 µg/ml and almost 90% cytotoxicity from 19.2 µg/ml upwards to 200 µg/ml.

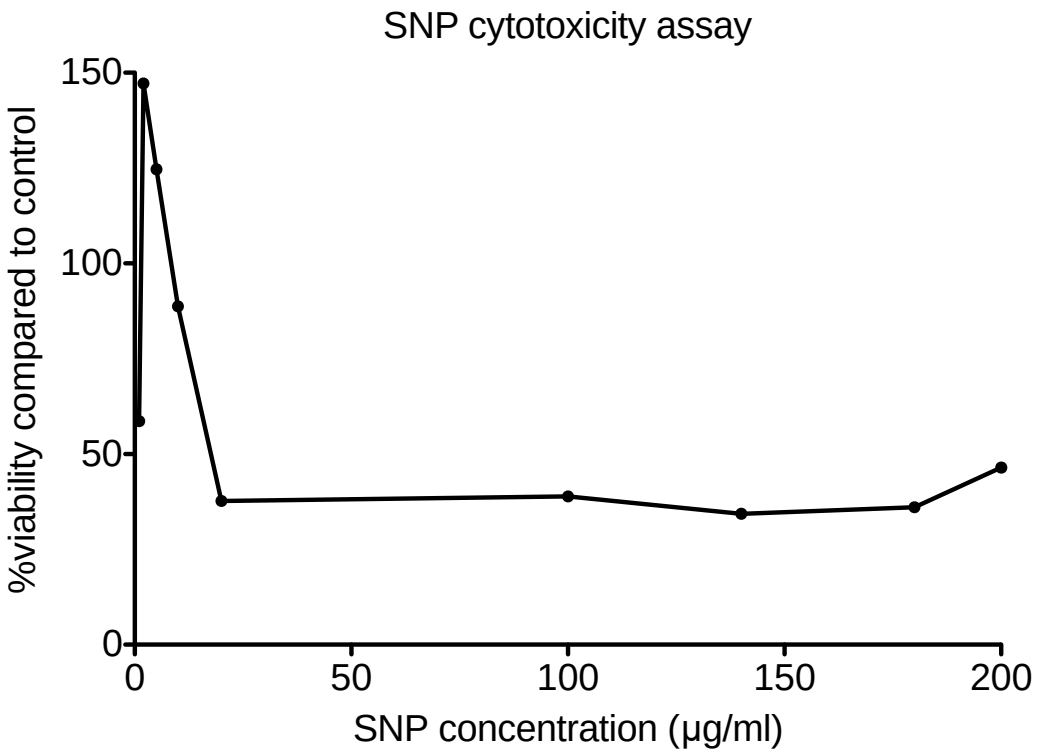

Fig 4.11 Cytotoxicity curve for silk nanoparticles applied to B16F10 cells in concentrations from 1 to 200 µg/ml. (n=1)

SNP cytotoxicity was determined using an MTT assay and applied to the assay in the same concentrations as for dextran and PEI. Cell viability of B16F10 cells after exposure to SNPs remains between 38 % and 43 % from 200 µg/ml to 20 µg/ml. Readings for cell viability spike to 147 % at 2 µg/ml and then drop to 58 % at 1 µg/ml. SNP IC50 is calculated at 17.85 µg/ml.

4.4 SNP characterization

Size (nm)	Polydispersity Index	Zeta Potential (mV)	Mobility μmcm/Vs
131	0.271	-34.6	-2.708

Table 4.1. Characteristics of silk nanoparticles as produced according to the protocol in materials and methods.

SNPs were characterised at a concentration of 200 μg/ml. SNP mean size is 131 nm in diameter, with a low polydispersity index (PDI) of 0.271. SNP zeta potential shows a negative zeta potential of -34.6 mV and an electrical mobility of -2.708 μm cm / Vs; all of which are consistent with previous findings for SNPs created using the same process (75).

4.5 Optimising homogenisation efficiency

Homogenisation or breakage efficiency was measured using LDH activity as a percentage of a 100 % control for all homogenates at each pass through the cell cracker. The data below showed breakage efficiency for the samples three, four and six. These data were selected as they were carried out according to the final optimised version of the protocol and hence most representative of the final experimental process.

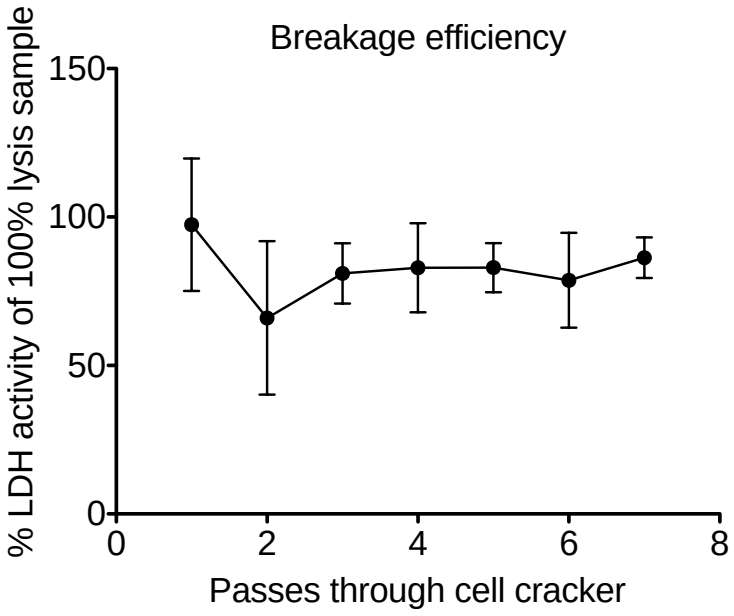

Fig 4.12 Homogenisation effieicncy at each pass of the homogenate through the cell cracker. Error bars represent standard deviation n=3.

Homogenisation efficiency remained high across all passes. Results shown are collated from three homogenates selected due to the quality of the data and differences in assay procedure from older homogenates due to optimisation.

Homogenisation efficiency was measured by comparing the LDH activity of each pass to that of a 100 % lysis control produced by the addition of Triton. The high initial value indicates a large proportion of homogenisation occouring on the first pass through the cell cracker.

4.6 Latent lysosomal activity

N-Acetyl-ß-glucosaminidase activity was used as a marker of lysosomal integrity. A sample was taken from the cell cracker at the end of each pass and

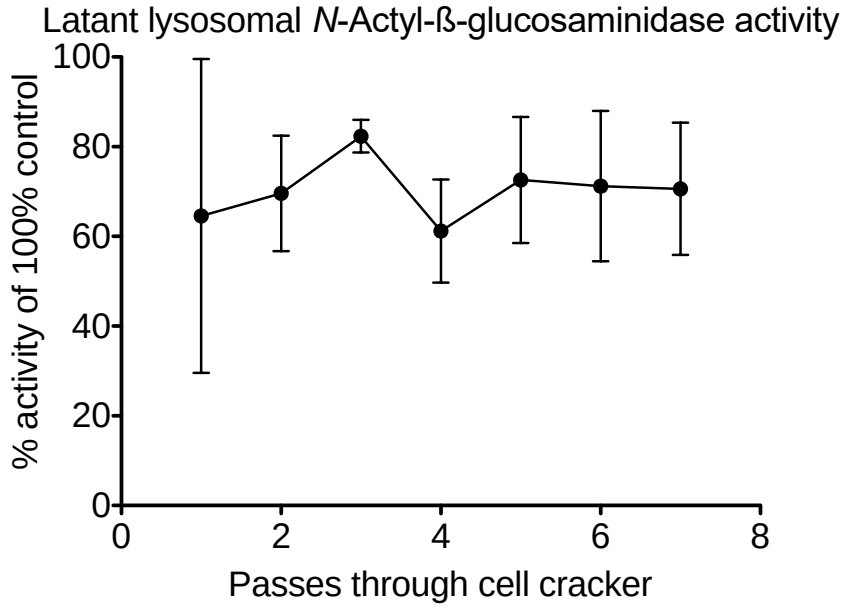

Fig 4.13 Plot of latent lysosomal activity as a marker of organelle preservation taken at each pass through the cell cracker.

The data shown is a collation of the data from the same three homogenates as used in determination of homogenisation efficiency, that they may inform each other. Lysosomal integrity varies widely, though remains bar the first pass though the cell cracker, above 50 %. Following the trend of the mean, the data show high integrity maintained over a large number of passes.

5 Discussion

Subcellular fractionation is an extremely powerful technique for quantifying the intracellular trafficking of macro- and nano-scale therapeutics. However, as stated before it requires a large degree of precision when selecting and validating the many required control experiments. Therefore the primary focus of this thesis was to establish a scheme of wet lab tested marker enzyme assays to be used to interrogate and assess future subcellular fractionations.

5.1 Optimisation of homogenisation

Acquiring a homogenate of high quality is vital to a successful fractionation given that the ideal homogenate contains a low percentage of intact cells but contains a high percentage of intact organelles.

Producing a homogenate of such high quality requires careful optimisation with regards to both these measures (112). The activity of the cytosolic enzyme LDH was used a marker for cell breakage, and to determine organelle integrity. Lysosomal integrity was measured using N-acetyl-ß-glucoseaminidase. Both were measured as a percentage of a 100 % lysis control produced via the addition of Triton X-100 to a sample from the same homogenisation pass.

Lysosomal integrity was used as a metric for organelle integrity, being the largest of the lysosomes and the mitochondria. Lysosomal integrity was measured comparing the activity of a sample from a given pass through a cell cracker with the activity of a sample taken from the same pass treated with the surfactant Triton X-100 to act a 100 % lysis control. Lysosomal integrity was assessed over a number of passes through the cell cracker. Integrity peaks at 80 % at pass three and remains consistently high over subsequent passes, showing that any damage occurs in the first few passes and no further damage occurs after pass number four. This closely mirrors published data in so far as high homogenisation is achieved while preserving organelle integrity (8). However, the published data using the same 7 μm clearance also show a lower immediate breakage by passes requiring upwards of twelve passes through the cell cracker in order to achieve adequate cell breakage (8), whereas the data presented here indicate high breakage efficiency by pass 2. The source of this disparity requires further investigation, given that the cells used were of the same line, cultured using the same process, and ultimately applied to the cell cracker in the same cellular concentration, having been resuspended in 2.5 times the pellet weight of PBS.

LDH activity as determined according to the materials and methods section (Fig.3.4), shows a large spike to almost 100 % efficiency after the first pass through the cell cracker and maintains an efficiency of over 80 % with the exclusion of pass two which shows an efficiency of 65 %. Given the high breakage efficiency within the first three to four passes through the cell cracker, optimal homogenisation was

observed well before pass four. This provides high homogenisation efficiency without subjecting the homogenate to too many passes and endangering organelle integrity.

LDH and N-acetyl-ß-glucoseaminidase activities, when taken together, show high breakage efficiency by pass three, coupled with high organelle integrity. This shows a need to pass the homogenate through the cell cracker no more than four times in order to produce a well homogenised suspension with high organelle integrity. Accordingly, all future experiments will be conducted with four passes through the cell cracker.

5.2 Optimisation of marker assays

The marker assays for B16F10 cells were selected based on previous studies (table 1.3) and the exclusivity of that enzyme to an intracellular compartment. The assays were examined and coordinated specifically to have no potential overlap with regards to substrates, products or co-enzymes and their exclusivity to the organelles to be detected.

5.2.1 Measuring specific activity

All enzyme activity was measured and expressed in terms of their specific activity with regards to the protein concentration of the homogenate used. This measurement was used specifically to keep a constant measurement across

varying concentrations of homogenate, as the output at the end of the homogenisation would vary due to the relatively gross methods used to prepare it. Therefore a measure of enzyme activity must be used which can account or the varying concentration of the homogenate. Measuring the protein concentration gives a good metric to use to determine concentration of the homogenate. However, protein concentration is not entirely representative of prior cell concentration and thus equals activity. Changes in the cytoskeleton and the effects of oxidative stress have been documented as changing the potential protein concentration of a cell, for example changes in the cytoskeleton (Welch, 1985).

5.2.2 Bicinchoninic acid (BCA) assay for homogenate protein concentration

Bicinchoninic acid (BCA) is a commonly used, highly accurate and quantitative assay for protein. As it was necessary to determine protein concentration in order to calculate the specific activity of certain enzymes, a BCA assay also known as the Peirce assay was used. Similar to the Lowry assay, the BCA assay relies on the well known biuret reaction, wherein peptides form a coloured chelate complex with copper ions (Cu^{2+}) (111). However, the BCA assay presents a distinct advantage over the Lowry assay in that it is less sensitive to compounds which may otherwise interfere with the reaction such as surfactants and denaturing agents.

The results of the BCA assay show a high protein content for samples one and two, after which it was determined to dilute the sample twofold in homogenisation buffer, in order for the readings to fall more comfortably within the bounds of the

standard curve. Samples 3-7 show a reasonably consistent concentration with a standard deviation of 0.2 over an average of 1.8. It is not imperative however that the protein concentration is consistent, as it is against this that DNA concentration and enzyme activity are normalised.

Individual replicates of the assay all show low standard deviation of 0.16 or lower with the exception of sample two, whose standard deviation is 0.28. This may be due in part to the fact that, as an undiluted sample, the assay itself produced an extremely deep colour, whose OD may have prevented an accurate reading from the equipment used.

5.2.3 Alkaline phosphatase specific activity

Alkaline phosphatase (ALP) (EC 3.1.3.1) is a hydrolase enzyme found in the plasma membrane, responsible dephosphorylation. It is a metallo-enzyme comprising three ions, typically two Zn^{2+} and one Mg^{2+} (Ghosh, 2013).

The plasma membrane is an important consideration when studying cellular internalisation of drugs (113). Being the largest barrier to cellular internalisation, drug uptake is often targeted towards overcoming this barrier, exploiting either transmembrane transport proteins and complexes (113), or endocytosis mechanisms (7). It is known that the surface charge of nanoparticles can alter their interaction with the plasma membrane of the cell and thus regulate uptake and internalisation (114). It is therefore important that we are able to gain an

understanding of the quantity of nanoparticles adhered to the plasma membrane and the proportion of these which are finally endocytosed.

ALP was chosen due to its abundance in the plasma membrane and specificity of its reaction, having no overlap with others in the battery of assays used. The assay for ALP was used as described by Rickwood (Rickwood, 1992) with no adaptation, as it was found to require suitably small amounts of homogenate sample.

The ALP assays for all homogenates show a high standard deviation within replicates, and a high variance across all assays run, with ANOVA showing a p-value of 0.014 (Fig 4.3). It is again difficult to compare the results with published values due to the much higher protein concentration in all homogenates produced, though it is doubtful that these results are representative of the true specific activity of ALP. Again, further work would be required in order to render results with a lower standard deviation and more consistent results between replicates.

5.2.4 Succinate dehydrogenase specific activity

Succinate dehydrogenase SDH (EC 1.3.5.1) is an enzyme complex bound exclusively to the inner mitochondrial membrane. It is often found in subcellular fractionation that the mitochondrial fraction has the propensity to contaminate the lysosomal fraction, due to their similar Stokes radius (115). This often results in significant overlap of the two fractions, potentially obfuscating the true destination of the carrier in question. The determination of anticancer drug delivery to the

mitochondria is also of particular interest, given their highly cytotoxic effects (116). The ability to target drug delivery to the mitochondria in cancer cells would be a valuable tool in increasing the efficacy of a drug.

The assay for SDH Involves the reduction of a tetrazolium salt (2-*p*-iodo-phenyl-3-*p*-nitrophenyl tetrazolium chloride) (INT) to a formazan dye in the presence of succinate, which can be quantified by comparison to a standard curve by measurement of optical density OD at 500nm (117).The method used was adapted from a published protocol (49). Optimisation for the amount of homogenate to be used proved trivial, as the process scales easily and as it is a colourimetric assay, the end product is relatively stable in comparison to fluorescence assays.

The values returned by the assay showed a low standard deviation over all by samples with the exception of samples four and five. The values cannot be compared to published data as they are taken from a homogenate exceeding the protein concentration of the published data (Fig 4.4) (Seib et al., 2006). However, despite the lack of comparable data, the consistency of the results show the assay scaled down successfully. Though the results themselves are within the bounds of statistical significance, a p-value of 0.43 is representative of approaching optimisation at the 5% significance level.

5.2.5 DNA concentration

DNA concentration was detected by means of a fluorescence assay using 4',6-diamidino-2-phenylindole (DAPI) as a dye.

The nucleus is of particular interest as a destination for nanoparticle based drug delivery, as it is a primary target for anticancer drug activity (118). One of the most common chemotherapeutic agents, doxorubicin's primary therapeutic action is the inhibition of DNA associated enzymes and intercalation (116). Similar activity is also observed in a number of other anticancer agents (119). It is therefore invaluable to be able to quantitatively assess the delivery of silk nanoparticles to the nucleus and their potential to accurately deliver a payload of DNA intercalating drugs.

DAPI is a faintly fluorescent compound used extensively as a DNA stain in fluorescence microscopy and forms a highly florescent compound when complexed with DNA. It shows a strong preference for A/T base pairs and polymerised DNA over denatured or degraded DNA (120). For this reason it is important to ensure the DNA sample used for the calibration curve contains a similar A/T base pair percentage as the intended sample. It is also important to maintain a pH of 7, as DAPI is subject to pH-dependent quenching (120). In order to reduce the effect of this, the methodology used to run the DAPI assay aimed to ensure a stable pH of 7 throughout the preparation and run time of the assay.

Optimisation of the DAPI assay was non-trivial, requiring many iterations before a suitable assay mixture was found. Secondly, it was found that the assay must be carried out using low binding DNA equipment, due to the small quantities of DNA being examined and the sensitivity of the assay.

The measured DNA concentration varied widely between homogenates and within replicates of the assays run (Fig 4.5). ANOVA testing between the samples revealed a p-value of 0.018. This suggests a significant difference either between the samples examined. This could possibly be explained by a fault in the methodology used to run the assay. It is evident that further optimisation is required in order to render a robust assay for nanogram quantities of DNA.

The reason for this variation requires further investigation, possibly with regards to DAPI's known pH dependent quenching (120), though as this was a known issue with the assay the pH was tightly regulated in the assay reagents in order to minimise the impact of this. Possible binding of the DNA to the 96 well plate or other equipment used in the preparation of the assay and therefore loss of fluorescence may also contribute towards the wide variation in readings. Lastly it is possible that preparing and conducting the assay in a darkroom could potentially reduce bleaching of the unbound DAPI prior to exposure to DNA and thus reduce the measured fluorescence.

5.2.6 Lactate dehydrogenase specific activity

LDH (EC 1.1.1.27) is a cytosolic enzyme, which facilitates the conversion of the final product of glycolysis, pyruvate, into lactate.

Cytosolic drug delivery is an effective method of introducing a drug to the intracellular compartments of a cancer cell. Often, the site of activity for anticancer drugs will be cytosolic organelles (121) and thus delivery to the cytosol enables greater access to the therapeutic targets. It is thus important to gain a quantitative insight into the amount of nanoparticles available in the cytosol in order to determine the availability of these nanoparticles to the organelles where they may be required.

As LDH is present in the cytosol of cells in large quantities, it is frequently used as a medical biomarker for tissue damage as a result of disease such as cancer or internal trauma including cardiac failure (Jaffe, 1996). LDH catalyses the conversions of pyruvate to and from lactate and relies on the presence of the co-enzyme NADH.

LDH was chosen as it is abundant in the cytosol and a well-established marker for cell damage, and thus the presence of a cytosolic fraction (Jaffe, 1996). The protocol used was adapted from the protocol proposed by Rickwood (Rickwood, 1992) and scaled down to be run in a 96 well plate. Optimisation for the LDH assay was required due to the speed of the reaction as measured by the decrease in OD

caused by the oxidation of NADH to NAD^+ and the limitations of the equipment used. Due to the maximum read rate available for number of samples run, it was only possible to read each reaction once every 10 seconds. The assay had to be scaled down in order to reduce reaction speed considerably to take readings over a time period of 10 min. Subsequently, the amount of sample used was reduced from 20 µl to 5 µl, reducing the reaction rate. Further optimisation of the assay in this regard was not needed.

The results from the assays run on the cellular homogenates show a high standard deviation over an average specific activity of 0.12 mM/mg/ml. Samples 2, 4 and 6 show consistency but there is no substantial significance to these results (Fig 3.3) given that there is such wide variation between homogenate and within replicates of each run. A p-value of 0.000 shows large variation over individual samples and a need to commit significant further work towards more effectively normalising the specific enzyme activity to the cellular protein content and developing a more robust method.

One possible reason for the large variation between samples is that the assay is conducted and then the activity calculated from the linear part of the absorbance curve produced by measuring the oxidation of NADH. This in turn limits the results to the area of the curve it was possible to capture, and if reading is delayed it is possible to miss part of the initial linear reaction period.

Secondly, it is possible that the activity is affected by the time between homogenate preparation and running the assay which can cause a reduction in enzyme activity due to proteases released from organelles such as the Golgi apparatus during homogenisation and the lysis stage of the assay.

5.2.7 N-acetyl-ß-glucosaminidase specific activity

The marker enzyme chosen for the lysosomal fraction was N-acetyl-ß-glucosaminidase (EC 3.2.1.50), due to its sequestration in lysosomes, and previous work showing its viability as a marker of lysosome stability (110). The assay used in this study, however, used Glycine-NaOH as a stopping buffer.

Lysosomotropic drug delivery has been demonstrated to offer an effective gateway into the cell for drugs adsorbed to the surface of silk nanoparticles (5). The drugs adsorbed to the SNP are released once the SNP is broken down inside the lysosome. Subcellular fractionation offers the opportunity to quantitatively explore the sequestration of SNPs into the lysosomal pathway, and thus the subsequent release of the adsorbed drug (5).

N-acetyl-ß-glucosaminidase acts as an exogylcosidase, which acts upon the non-reducing end of N-acetyl-D-glucosamine residues in heparin sulphate. This activity allows it to liberate 4-methylumbelliferone from 4-methylumbelliferyl N-acetyl-ß-D-glucosaminide (110). Following the reaction, the liberated 4-

methylumbelliferone can be quantitatively assessed by measurement of its fluorescence and comparing this against a calibration curve.

The lysosomal N-acetyl-ß-glucoseaminidase assay, while well documented (110), proved difficult to optimise correctly for the cell line and volumes. It was found that while a one minute reaction time was sufficient for the assay, prior incubation in a solution of 0.5 % Triton TX-100 in homogenisation buffer was required to disrupt the lysosomal membrane and make available the entire activity of N-acetyl-ß-glucoseaminidase in the sample. The problem was addressed following carrying out the assay with increasingly high concentrations of Triton TX-100, and seeing a limited response, and so a prior incubation time of 3 min with a 0.5 % solution of Triton TX-100 was tried.

Another study investigated a possible quenching effect and found that the maximum value, which could reliably be detected without quenching, was 250 µM (data not shown), which was beyond the maximum concentration used to produce the standard curve (50 µM) and so this possibility could be ruled out.

The data shown in the results section (Fig 4.7) show consistent results for homogenates from only one run of the assay. Though the intent was to conduct a further two replicates of the assay for each sample, the work was severely limited by time constraints. As such it is unwise to draw too many conclusions from the data presented.

The negative results for samples 6 and 7 are due to the fact that the values returned from the assay are too low to fall on the calibration curve and so the calculation applied returns an incorrect value. In response, the assay will be run for a longer time interval, taking care to not run the assay to completion and the larger value applied to the calibration curve and the specific activity determined, taking into account the longer time interval used.

5.3 Characterisation of silk nanoparticles

Before applying the SNPs to an assay or tissue culture, it is important to characterise them and ensure they are correctly formed with regards to previous published data

The results shown agree with previously characterised particles produced using the same method (Seib et al., 2013). The characterisation of the SNPs produced showed properties consistent with previously published data (Seib et al., 2013) with the only marked difference being an increase in particle size at 131 nm diameter over the published data of 100 nm.

5.4 Cytotoxicity of silk nanoparticles

Before assessing the cytotoxicity of silk nanoparticles, it was necessary to have a good model for the cell behaviour in response to uptake of a non-cytotoxic polymer (dextran) and a cytotoxic polymer (PEI) at varying concentrations.

The negative control conducted with dextran showed high cell viability over all dextran concentrations, thought the standard deviation for the data points is high, the trend for the mean values of each data point is linear (Fig 3.8). This serves as a reliable negative control.

The positive control was conducted with PEI, known to be cytotoxic (Fischer, 2003), and showed a high cytotoxicity with over 90 % cytotoxicity from 19.2 μg/ml upwards to 200 μg/ml and an IC50 value of 8.8 μg/ml (Fig 3.9). The high cytotoxicity of PEI allows it to serve as a good positive control for cell viability under exposure to polymers taken up by endocytosis.

A cytotoxicity assay was undertaken using silk nanoparticles in the same concentrations as dextran and PEI. The results show widely varying cytotoxicity, and a cell viability well below previously published data for SNPs produced using the same methods (Seib et al., 2013) which found SNPs to possess an IC50 of greater than 120μg/ml. This may be due to the fact that the results are not normalised against a control which takes into account the varying dilutions, made to the media in order to vary the concentration of nanoparticles present. Future work will involve an SNP cytotoxicity assay which accounts for the dilution factor used in the application of SNPs.

5.5 Choice of cell line

The cell line B16F10 was used in all experiments due to the fact that it is a well-documented cell line with well characterised responses to therapeutic agents and have also previously been used in similar fractionation studies (8). Furthermore, B16F10 cells have been used previously to screen for and move therapeutics from the laboratory to the clinic (Seymore, 1994, Jones, 2006, Rademaker-Lakhai, 2004).

5.6 Future work

Future work should include an initial fractionation study in order to optimise the techniques used in producing; isolating and interrogating the individual fractions from a cellular homogenate. These studies will be conducted without the presence of silk nanoparticles in the cell culture media, in order to refine the methods used for future work.

Of course, the limitations of this method as discussed in the introduction are relevant. Fractionation requires careful optimisation when producing a functioning protocol, and so special attention will be paid to this.

A second round of experiments will examine the trafficking of SNPs using a fractionation scheme optimised in the initial study and will examine the trafficking

at three time points, 0 hours, 4 hours, 24 hours and every 24 hours following for 5 days. These time points are chosen based on the practicality of taking readings, and on previous work by Seib *et al* (Seib FP 2006) on the rate of polymer uptake in B16F10 cells.

The SNPs may be radio-tagged with deuterium using hydrogen-deutrium exchange, which is easily applied to amine groups or the backbone of a protein. It can also be done at neutral pH and in aqueous phase, meaning the risk of altering the SNPs is low. However, this presents its own difficulties. The SNPs, in order to maintain the original level of labelling, must be kept in an aprotic environment, or the labelling may become slowly quenched. This is impossible in the context of cell culture and endosomotropic delivery, and to the quenching must be accounted for.
However, it is possible to label silk with deuterium by way of antibody radiolabeling with monoclonal antibodies. The monoclonal antibodies themselves can lend high thermodynamic stability to the radiolabel, and may be applied directly to the SNPs, circumventing the need for time and resource intensive sericulture, though quenching is still an issue on this case, and so another more stable isotope may be used, such as iodine 125^{+} ($^{125}I^{+}$).
Asakura proposed a method of deuterium labelling silk (Asakura, 1997). This method involves rearing silkworms to the fifth instar, and feeding them an artificial diet rich in deuterium-labelled glycine, before pupation. This results in deuterium being evenly disbursed through the silk fibres in glycine rich regions.

The limitations of this are obvious. Sericulture is a very labour intensive method, and is time consuming to optimise. However, it does allow very fine control over deuterium concentration and thus optimisation of the process to the fractionation scheme in use is done with relative ease.

Supplementary experiments will include fluorescence microscopy of cells at a number of time points following incubation with silk nanoparticles. Based on previous studies, it is known that such nanoparticles preferentially accumulate in late endosomes and lysosomes (Seib FP 2006). To this end imaging will be conducted by staining lysosomes with the dye LysoBrite Red, and the silk nanoparticles will be labelled with Alexa Flour 488, due to its high photostability and vivid green fluorescence in contrast to LysoBrite Red. An immunofluorescence approach may be used to tag SNPs, however it is possible that this may change the pharmacokinetics of the nanoparticle itself.

Fluorescence microscopy has two major flaws in the context of quantitatively tracing the fate of SNPs. Primarily, it is a qualitative process, not being able to determine direct abundance of a marker, it can only facilitate estimation by relative fluorescence. Secondly, being a fluorescence based methodology, it relies on fluorescent probes, which are subject to quenching under exposure to one or more conditions including natural and artificial light, pH, pressure and temperature.

Finally there is a need to fix a cell, unless live cell imaging is being used, and this in some cases can affect the appearance of the image collected. It is important to maintain stringent fixing protocols so as not to damage any of the cellular ultrastructure or organelles. Live cell imaging may also be used to circumvent this problem, and also give us a time dependent map of SNP trafficking over various time points.

Finally, the greatest drawback of microscopy is that it has an extremely low sample size, being very low throughput (one cell at a time) in comparison to fractionation, which can process whole tissues at once.

Despite these drawbacks, fluorescence microscopy when used appropriately can be a useful tool to corroborate the findings of a fractionation study, and inform future work to more finely interrogate fractions containing organelles where fluorescence is observed.

The cytotoxicity of SNPs loaded with doxorubicin will be determined in the same manner as unloaded particles at the same nanoparticle concentrations.

Drug loading and release will the object of separate study in order to determine dosage for the application of nanoparticles. Doxorubicin will be used due to the fact that it is well documented and have been used extensively in similar studies. Second to this is the fact that with regards to a drug loading and release study, doxorubicin whether released or in excess is easily quantified by way of its

fluorescence. This allows a release or loading study to be carried out with very little other specialised equipment.

6 References

1. Diab T, Pritchard EM, Uhrig BA, Boerckel JD, Kaplan DL, Guldberg RE. A silk hydrogel-based delivery system of bone morphogenetic protein for the treatment of large bone defects. J Mech Behav Biomed Mater. 2012;11:123–31.

2. Karageorgiou V, Tomkins M, Fajardo R, Meinel L, Snyder B, Wade K, et al. Porous silk fibroin 3-D scaffolds for delivery of bone morphogenetic protein-2 in vitro and in vivo. J Biomed Mater Res A. 2006;78(2):324–334.

3. Kundu J, Chung Y-I, Kim YH, Tae G, Kundu SC. Silk fibroin nanoparticles for cellular uptake and control release. Int J Pharm. 2010;388(1–2):242–50.

4. Tsioris K, Raja WK, Pritchard EM, Panilaitis B, Kaplan DL, Omenetto FG. Fabrication of Silk Microneedles for Controlled-Release Drug Delivery. Adv Funct Mater. 2012;22(2):330–5.

5. Seib FP, Jones GT, Rnjak-Kovacina J, Lin Y, Kaplan DL. pH-dependent anticancer drug release from silk nanoparticles. Adv Heal Mater. 2013;2(12):1606–1611.

6. Duncan R. Polymer conjugates for tumour targeting and intracytoplasmic delivery. The EPR effect as a common gateway? Pharm Sci Technol Today. 1999;2(11):441–449.

7. Zhang S, Gao H, Bao G. Physical Principles of Nanoparticle Cellular Endocytosis. ACS Nano. 2015;9(9):8655–71.

8. Seib FP, Jones AT, Duncan R. Establishment of subcellular fractionation techniques to monitor the intracellular fate of polymer therapeutics I. Differential centrifugation fractionation B16F10 cells and use to study the intracellular fate of HPMA copolymer - doxorubicin. J Drug Target. 2006;14(6):375–390.

9. de Duve C, Pressman B, Gianetto R, Wattiaux R, Appelmans F. Tissue fractionation studies. 6. Intracellular distribution patterns of enzymes in rat-liver tissue. Biochem J. 1955;60(4):604.

10. Carragee EJ, Hurwitz EL, Weiner BK. A critical review of recombinant human bone morphogenetic protein-2 trials in spinal surgery: emerging safety concerns and lessons learned. Spine J. 2011;11(6):471–491.

11. Vepari C, Kaplan DL. Silk as a Biomaterial. Prog Polym Sci. 2007;32(8–9):991–1007.

12. Omenetto FG, Kaplan DL. New opportunities for an ancient material. Science. 2010;329(5991):528–31.

13. Lefèvre T, Boudreault S, Cloutier C, Pézolet M. Diversity of molecular transformations involved in the formation of spider silks. J Mol Biol. 2011;405(1):238–253.

14. Dams-Kozlowska H, Majer A, Tomasiewicz P, Lozinska J, Kaplan DL, Mackiewicz A. Purification and cytotoxicity of tag-free bioengineered spider silk proteins. J Biomed Mater Res A. 2013;101(2):456–64.

15. Numata K, Subramanian B, Currie HA, Kaplan DL. Bioengineered silk protein-based gene delivery systems. Biomaterials. 2009;30(29):5775–5784.

16. Wenk E, Merkle HP, Meinel L. Silk fibroin as a vehicle for drug delivery applications. J Control Release. 2011;150(2):128–141.

17. Kataoka K, Matsumoto T, Yokoyama M, Okano T, Sakurai Y, Fukushima S, et al. Doxorubicin-loaded poly (ethylene glycol)–poly (β-benzyl-l-aspartate) copolymer micelles: their pharmaceutical characteristics and biological significance. J Control Release. 2000;64(1–3):143–153.

18. Monsuez J-J, Charniot J-C, Vignat N, Artigou J-Y. Cardiac side-effects of cancer chemotherapy. Int J Cardiol. 2010;144(1):3–15.

19. Hortobagyi GN. Anthracyclines in the treatment of cancer. Drugs. 1997;54(Suppl 4):1–7.

20. Carmeliet P, Jain RK. Angiogenesis in cancer and other diseases. Nature. 2000;407(6801):249–257.

21. Zhang W, Wang X, Wang S, Zhao J, Xu L, Zhu C, et al. The use of injectable sonication-induced silk hydrogel for VEGF165 and BMP-2 delivery for elevation of the maxillary sinus floor. Biomaterials. 2011;32(35):9415–9424.

22. Wu P, Liu Q, Li R, Wang J, Zhen X, Yue G, et al. Facile preparation of paclitaxel loaded silk fibroin nanoparticles for enhanced antitumor efficacy by locoregional drug delivery. ACS Appl Mater Interfaces. 2013;5(23):12638–12645.

23. Whang K, Tsai DC, Nam EK, Aitken M, Sprague SM, Patel PK, et al. Ectopic bone formation via rhBMP-2 delivery from porous bioabsorbable polymer scaffolds. J Biomed Mater Res. 1998;42(4):491–499.

24. DeMuth PC, Min Y, Irvine DJ, Hammond P. T. Implantable Silk Composite Microneedles for Programmable Vaccine Release Kinetics and Enhanced Immunogenicity in Transcutaneous Immunization. Adv Heal Mater. 2014;3(1):47–58.

25. Wang X, Yucel T, Lu Q, Hu X, Kaplan DL. Silk nanospheres and microspheres from silk/pva blend films for drug delivery. Biomaterials. 2010;31(6):1025–1035.

26. Seib FP, Pritchard EM, Kaplan DL. Self-Assembling Doxorubicin Silk Hydrogels for the Focal Treatment of Primary Breast Cancer. Adv Funct Mater. 2013;23(1):58–65.

27. Raja WK, Maccorkle S, Diwan IM, Abdurrob A, Omenetto FG, Kaplan DL. Transdermal delivery devices: Fabrication, mechanics and drug release from silk. Small. 2013;9(21):3704–3713.

28. Zhang W, Zhu C, Ye D, Xu L, Zhang X, Wu Q, et al. Porous silk scaffolds for delivery of growth factors and stem cells to enhance bone regeneration. Pandit A, editor. PLoS ONE [Internet]. 2014;9(7). Available from: http://dx.plos.org/10.1371/journal.pone.0102371

29. Chao P-HG, Yodmuang S, Wang X, Sun L, Kaplan DL, Vunjak-Novakovic G. Silk hydrogel for cartilage tissue engineering. J Biomed Mater Res B Appl Biomater. 2010;95(1):84–90.

30. Koh L-D, Cheng Y, Teng C-P, Khin Y-W, Loh X-J, Tee S-Y, et al. Structures, mechanical properties and applications of silk fibroin materials. Prog Polym Sci. 2015;46:86–110.

31. Wang X, Tian J, Yong K-T, Zhu X, Lin MC-M, Jiang W, et al. Immunotoxicity assessment of CdSe/ZnS quantum dots in macrophages, lymphocytes and BALB/c mice. J Nanobiotechnology [Internet]. 2016 [cited 2016 Sep 16];14(10). Available from: http://www.jnanobiotechnology.com/content/14/1/10

32. Barenholz Y (Chezy). Doxil® — The first FDA-approved nano-drug: Lessons learned. J Control Release. 2012;160(2):117–34.

33. Fox JL. FDA advisors okay NeXstar's DaunoXome. Nat Biotechnol. 1995;13(7):635–6.

34. Carnevale J, Ko AH. MM-398 (nanoliposomal irinotecan): emergence of a novel therapy for the treatment of advanced pancreatic cancer. Future Oncol. 2016;12(4):453–64.

35. Anselmo AC, Mitragotri S. Nanoparticles in the clinic. Bioeng Transl Med. 2016;1(1):10–29.

36. Panilaitis B, Altman GH, Chen J, Jin HJ, Karageorgiou V, Kaplan DL. Macrophage responses to silk. Biomaterials. 2003;24(18):3079–3085.

37. Belhaj Khalifa I, Ladhari N, Touay M. Application of sericin to modify textile supports. J Text Inst. 2012;103(4):370–7.

38. Inoue S, Tanaka K, Arisaka F, Kimura S, Ohtomo K, Mizuno S. Silk fibroin of Bombyx mori is secreted, assembling a high molecular mass elementary unit consisting of H-chain, L-chain, and P25, with a 6:6:1 molar ratio. J Biol Chem. 2000;275(51):40517–28.

39. Zhou C-Z, Confalonieri F, Medina N, Zivanovic Y, Esnault C, Yang T, et al. Fine organisation of the Bombyx mori fibroin heavy chain gene. Nucleic Acids Res. 2000;28(12):2413–9.

40. Altman GH, Diaz F, Jakuba C, Calabro T, Horan RL, Chen J, et al. Silk-based biomaterials. Biomaterials. 2003;24(3):401–416.

41. Liu X, Zhang K-Q. Silk Fiber — Molecular Formation Mechanism, Structure-Property Relationship and Advanced Applications. In: Lesieur C, editor. Oligomerization of Chemical and Biological Compounds [Internet]. InTech; 2014. Available from: http://www.intechopen.com/books/oligomerization-of-chemical-and-biological-compounds/silk-fiber-molecular-formation-mechanism-structure-property-relationship-and-advanced-applications

42. Zhou C-Z, Confalonieri F, Jacquet M, Perasso R, Li Z-G, Janin J. Silk fibroin: structural implications of a remarkable amino acid sequence. Proteins. 2001;44(2):119–122.

43. Asakura T, Ashida J, Yamane T, Kameda T, Nakazawa Y, Ohgo K, et al. A Repeated β-Turn Structure in Poly(Ala-Gly) as a Model for Silk I of Bombyx mori Silk Fibroin studied with Two-dimensional Spin-diffusion NMR under off Magic Angle Spinning and Rotational Echo Double Resonance. J Mol Biol. 2001;306(2):291–305.

44. Asakura T, Sugino R, Okumura T, Nakazawa Y. The role of irregular unit, GAAS, on the secondary structure of Bombyx mori silk fibroin studied with 13C CP/MAS NMR and wide-angle X-ray scattering. Protein Sci. 2002;11(8):1873–7.

45. Shen Y, Johnson MA, Martin DC. Microstructural Characterization of Bombyx mori Silk Fibers. Macromolecules. 1998;31(25):8857–64.

46. Wilson D, Valluzzi R, Kaplan D. Conformational transitions in model silk peptides. Biophys J. 2000;78(5):2690–2701.

47. Cheng Y, Koh L-D, Li D, Ji B, Han M-Y, Zhang Y-W. On the strength of β-sheet crystallites of Bombyx mori silk fibroin. J R Soc Interface [Internet]. 2014;11(96). Available from: http://rsif.royalsocietypublishing.org/cgi/doi/10.1098/rsif.2014.0305

48. Timár-Balázsy Á, Eastop D. Chemical principles of textile conservation. Oxford [etc.] : Butterworth-Heinemann; 1998. (Butterworth-Heinemann series in conservation and museology).

49. Padamwar MN, Pawar AP. Silk sericin and its applications: A review. J Sci Ind Res India. 2004;63(4):323–329.

50. Zhang X, Khan MM, Yamamoto T, Tsukada M, Morikawa H. Fabrication of silk sericin nanofibers from a silk sericin-hope cocoon with electrospinning method. Int J Biol Macromol. 2012;50(2):337–347.

51. Gamo T, Maruyama G. A simple method for the measurement of low levels of serum IgE. Clin Allergy. 1977;7(6):597–604.

52. Chen X, Shao Z, Knight DP, Vollrath F. Conformation transition kinetics of Bombyx mori silk protein. Proteins. 2007;68(1):223–31.

53. Asakura T, Okushita K, Williamson MP. Analysis of the Structure of Bombyx mori Silk Fibroin by NMR. Macromolecules. 2015;48(8):2345–57.

54. Kratky O, Schauenstein E, Sekora A. An Unstable Lattice in Silk Fibroin. Nature. 1950;165(7):319–320.

55. Morozova-Roche LA, Zamotin V, Malisauskas M, Öhman A, Chertkova R, Lavrikova MA, et al. Fibrillation of Carrier Protein Albebetin and Its Biologically Active Constructs. Multiple Oligomeric Intermediates and Pathways. Biochemistry (Mosc). 2004;43(30):9610–9.

56. Valluzzi R, Gido SP, Muller W, Kaplan DL. Orientation of silk III at the air-water interface. Int J Biol Macromol. 1999;24(2–3):237–242.

57. Hino T, Tanimoto M, Shimabayashi S. Change in secondary structure of silk fibroin during preparation of its microspheres by spray-drying and exposure to humid atmosphere. J Colloid Interface Sci. 2003;266(1):68–73.

58. Mandal BB, Kundu SC. Self-assembled silk sericin/poloxamer nanoparticles as nanocarriers of hydrophobic and hydrophilic drugs for targeted delivery. Nanotechnology [Internet]. 2009;20(35). Available from: http://stacks.iop.org/0957-4484/20/i=35/a=355101?key=crossref.bd6d2b164044c4b037ca780748f3c71c

59. Rickwood D. Preparative Centrifugation: A Practical Approach. IRL Press at Oxford University Press; 1992. (Practical Approach; vol. 113).

60. Meinel L, Hofmann S, Karageorgiou V, Kirker-Head C, McCool J, Gronowicz G, et al. The inflammatory responses to silk films in vitro and in vivo. Biomaterials. 2005;26(2):147–55.

61. Soong HK, Kenyon KR. Adverse Reactions to Virgin Silk Sutures in Cataract Surgery. Ophthalmology. 1984;91(5):479–83.

62. Liu H, Ge Z, Wang Y, Toh SL, Sutthikhum V, Goh JCH. Modification of sericin-free silk fibers for ligament tissue engineering application. J Biomed Mater Res B Appl Biomater. 2007;82(1):129–38.

63. Horan RL, Antle K, Collette AL, Wang Y, Huang J, Moreau JE, et al. In vitro degradation of silk fibroin. Biomaterials. 2005;26(17):3385–93.

64. Li M, Ogiso M, Minoura N. Enzymatic degradation behavior of porous silk fibroin sheets. Biomaterials. 2003;24(2):357–365.

65. Colilla M, Baeza A, Vallet-Regí M. Mesoporous silica nanoparticles for drug delivery and controlled release applications. In: Levy D, Zayat M, editors. The Sol-Gel Handbook-Synthesis, Characterization, and Applications: Synthesis, Characterization and Applications, 3-Volume Set. 1st ed. Weinheim, Germany: Wiley-VCH Verlag GmbH & Co; 2015. p. 1309–1344.

66. Hadziyannis SJ, Sette HJ, Morgan TR, Balan V, Diago M, Marcellin P, et al. Peginterferon-alpha2a and ribavirin combination therapy in chronic hepatitis C: a randomized study of treatment duration and ribavirin dose. Ann Intern Med. 2004;140(5):346–355.

67. Li LZ, Zhou DM, Peijnenburg WJ, van Gestel CA, Jin SY, Wang YJ, et al. Toxicity of zinc oxide nanoparticles in the earthworm, Eisenia fetida and subcellular fractionation of Zn. Env Int. 2011;37(6):1098–104.

68. Sun C, Lee JS, Zhang M. Magnetic nanoparticles in MR imaging and drug delivery. Adv Drug Deliv Rev. 2008;60(11):1252–65.

69. Lovrić J, Bazzi HS, Cuie Y, Fortin GRA, Winnik FM, Maysinger D. Differences in subcellular distribution and toxicity of green and red emitting CdTe quantum dots. J Mol Med Berl. 2005;83(5):377–85.

70. Ishida T, Wang X, Shimizu T, Nawata K, Kiwada H. PEGylated liposomes elicit an anti-PEG IgM response in a T cell-independent manner. J Control Release. 2007;122(3):349–55.

71. Marchal S, El Hor A, Millard M, Gillon V, Bezdetnaya L. Anticancer Drug Delivery: An Update on Clinically Applied Nanotherapeutics. Drugs. 2015;75(14):1601–11.

72. Awada A, Garcia AA, Chan S, Jerusalem GHM, Coleman RE, Huizing MT, et al. Two schedules of etirinotecan pegol (NKTR-102) in patients with previously treated metastatic breast cancer: a randomised phase 2 study. Lancet Oncol. 2013;14(12):1216–25.

73. Slingerland M, Guchelaar H-J, Gelderblom H. Liposomal drug formulations in cancer therapy: 15 years along the road. Drug Discov Today. 2012;17(3–4):160–6.

74. Kan P. A brief review on development of liposome in Taiwan. J Med Biol Eng. 2007;27(1):53–6.

75. Leonard RCF, Williams S, Tulpule A, Levine AM, Oliveros S. Improving the therapeutic index of anthracycline chemotherapy: Focus on liposomal doxorubicin (Myocet™). Breast. 2009;18(4):218–24.

76. Frampton JE. Mifamurtide: a review of its use in the treatment of osteosarcoma. Paediatr Drugs. 2010;12(3):141–153.

77. Auerbach M, Ballard H. Clinical use of intravenous iron: administration, efficacy, and safety. Hematology. 2010;2010:338–47.

78. Panowski S, Bhakta S, Raab H, Polakis P, Junutula JR. Site-specific antibody drug conjugates for cancer therapy. MAbs. 2014;6(1):34–45.

79. Miller KD, Dieras V, Harbeck N, Andre F, Mahtani RL, Gianni L, et al. Phase IIa Trial of Trastuzumab Emtansine With Pertuzumab for Patients With Human Epidermal Growth Factor Receptor 2–Positive, Locally Advanced, or Metastatic Breast Cancer. J Clin Oncol. 2014;32(14):1437–44.

80. Zhang Y-Q, Shen W-D, Xiang R-L, Zhuge L-J, Gao W-J, Wang W-B. Formation of silk fibroin nanoparticles in water-miscible organic solvent and their characterization. J Nanopart Res. 2007;9(5):885–900.

81. Rivera Gil P, Hühn D, del Mercato LL, Sasse D, Parak WJ. Nanopharmacy: Inorganic nanoscale devices as vectors and active compounds. Pharmacol Res. 2010;62(2):115–25.

82. Maeda H, Matsumura Y. Tumoritropic and lymphotropic principles of macromolecular drugs. Crit Rev Ther Drug Carrier Syst. 1989;6(3):193—210.

83. Thiebaut F, Tsuruo T, Hamada H, Gottesman MM, Pastan I, Willingham MC. Cellular localization of the multidrug-resistance gene product P-glycoprotein in normal human tissues. Proc Natl Acad Sci. 1987;84(21):7735–7738.

84. Saheki Y, De Camilli P. Synaptic Vesicle Endocytosis. Cold Spring Harb Perspect Biol [Internet]. 2012;4(9). Available from: http://cshperspectives.cshlp.org/lookup/doi/10.1101/cshperspect.a005645

85. Simons M, Raposo G. Exosomes – vesicular carriers for intercellular communication. Curr Opin Cell Biol. 2009;21(4):575–81.

86. Gordon S. Pattern recognition receptors: doubling up for the innate immune response. Cell. 2002;111(7):927–930.

87. Setty SRG, Tenza D, Truschel ST, Chou E, Sviderskaya EV, Theos AC, et al. BLOC-1 is required for cargo-specific sorting from vacuolar early endosomes toward lysosome-related organelles. Mol Biol Cell. 2007;18(3):768–780.

88. Kiss AL. Caveolae and the regulation of endocytosis. Adv Exp Med Biol. 2012;729:14–28.

89. McMahon HT, Boucrot E. Molecular mechanism and physiological functions of clathrin-mediated endocytosis. Nat Rev Mol Cell Biol. 2011;12(8):517–33.

90. Michael Danielsen E, Hansen GH. Small molecule pinocytosis and clathrin-dependent endocytosis at the intestinal brush border: Two separate pathways into the enterocyte. Biochim Biophys Acta. 2016;1858(2):233–43.

91. Gao H, Shi W, Freund LB. Mechanics of receptor-mediated endocytosis. Proc Natl Acad Sci U A. 2005;102(27):9469–9474.

92. Tauber AI. Metchnikoff and the phagocytosis theory. Nat Rev Mol Cell Biol. 2003;4(11):897–901.

93. Godlee C, Kaksonen M. From uncertain beginnings: Initiation mechanisms of clathrin-mediated endocytosis. J Cell Biol. 2013;203(5):717–25.

94. Huang F, Khvorova A, Marshall W, Sorkin A. Analysis of clathrin-mediated endocytosis of epidermal growth factor receptor by RNA interference. J Biol Chem. 2004;279(16):16657–16661.

95. Lamaze C, Schmid S. The emergence of clathrin-independent pinocytic pathways. Curr Opin Cell Biol. 1995;7(4):573–80.

96. Vieira AV, Lamaze C, Schmid SL. Control of EGF receptor signaling by clathrin-mediated endocytosis. Science. 1996;274(5295):2086–9.

97. Bareford LM, Swaan PW. Endocytic mechanisms for targeted drug delivery. Adv Drug Deliv Rev. 2007;59(8):748–758.

98. Rothberg KG, Heuser JE, Donzell WC, Ying YS, Glenney JR, Anderson RG. Caveolin, a protein component of caveolae membrane coats. Cell. 1992;68(4):673–682.

99. Parton RG, Del Pozo D. Caveolae as plasma membrane sensors, protectors and organizers. Nat Rev Mol Cell Biol. 2013;14:98–112.

100. Conner SD, Schmid SL. Regulated portals of entry into the cell. Nature. 2003;422(6927):37–44.

101. Kasahara K, Nakayama Y, Kihara A, Matsuda D, Ikeda K, Kuga T, et al. Rapid trafficking of c-Src, a non-palmitoylated Src-family kinase, between the plasma membrane and late endosomes/lysosomes. Exp Cell Res. 2007;313(12):2651–66.

102. Kasahara K, Nakayama Y, Sato I, Ikeda K, Hoshino M, Endo T, et al. Role of Src-family kinases in formation and trafficking of macropinosomes. J Cell Physiol. 2007;211(1):220–32.

103. Dahm R. From discovering to understanding. EMBO Rep. 2010;11(3):153–160.

104. Bensley RR. On the fat distribution in mitochondria of the guinea pig liver. Anat Rec. 1937;69(3):341–353.

105. Claude A. The Constitution of Mitochondria and Microsomes, and the Distribution of Nucleic Acid in the Cytoplasm of a Leukemic Cell. J Exp Med. 1944;80(1):19–29.

106. Claude A, Fullam EF. An Electron Microscope Study of Isolated Mitochondria : Method and Preliminary Results. J Exp Med. 1945;81(1):51–62.

107. Hogeboom GH. Fractionation of cell components of animal tissue. In: Methods in Enzymology. Academic PRess; 1955. p. 16–19.

108. Claude A. Distribution of nucleic acids within the cell and the morphological constitution of cytoplasm. Biol Symp. 1943;10:111–129.

109. Zhao HEA, Ruberu K, Li H, Garner B. Analysis of subcellular [57Co] cobalamin distribution in SH-SY5Y neurons and brain tissue. J Neurosci Methods. 2013;217(1–2):67–74.

110. Crémazy A, Levy JL, Campbell PG, Fortin C. Uptake and subcellular partitioning of trivalent metals in a green alga: comparison between Al and Sc. Biometals. 2013;26(6):989–1001.

111. Blackman MJEA, Bannister LH. Apical organelles of Apicomplexa: biology and isolation by subcellular fractionation. Mol Biochem Parasitol. 2001;117(1):11–25.

112. Carlsjohn EEA, Nyström J, Karlsson H, Svennerholm AM, Nilsson CL. Characterization of the Outer Membrane Protein Profile from Disease-Related Helicobacter p ylori Isolates by Subcellular Fractionation and Nano-LC FT-ICR MS Analysis. J Proteome Res. 2006;5(11):3197–3204.

113. Peters TJ, De Duve C. Lysosomes of the arterial wall. II. Subcellular fractionation of aortic cells from rabbits with experimantal atheroma. Exp Mol Pathol. 1974;20(2):228–56.

114. Vassault. Methods of enzymatic analysis, enzymes I: Oxidoreductases, transferases. 1983;Vol. III:118–26.

115. Klemm AR, Young D, Llyod JB. Effects of polyethylimine on endocytosis and lysosomal stability. Biochem Pharmacol. 1998;56(1):41–46.

116. Walker JM, editor. The protein protocols handbook. 2nd ed. Totowa, N.J: Humana Press; 2002. 1146 p.

117. Lavoie M, Bernier J, Fortin C, Campbell PG. Cell homogenization and subcellular fractionation in two phytoplanktonic algae: implications for the assessment of metal subcellular distributions. Limnol Oceanogr Methods. 2009;7(4):277–286.

118. Saito G, Swanson JA, Lee K-D. Drug delivery strategy utilizing conjugation via reversible disulfide linkages: role and site of cellular reducing activities. Adv Drug Deliv Rev. 2003;55(2):199–215.

119. Arvizo RR, Miranda OR, Thompson MA, Pabelick CM, Bhattacharya R, Robertson JD, et al. Effect of Nanoparticle Surface Charge at the Plasma Membrane and Beyond. Nano Lett. 2010 Jul 14;10(7):2543–8.

120. Musálková D, Lukás J, Majer F, Hrebícek O, Svobodová E, Kuchar L, et al. Rapid Isolation of Lysosomal Membranes from Cultured Cells. Folia Biol (Praha). 2013;59(1):41.

121. Tacar O, Sriamornsak P, Dass CR. Doxorubicin: an update on anticancer molecular action, toxicity and novel drug delivery systems: Doxorubicin cell and molecular biological activity. J Pharm Pharmacol. 2013 Feb;65(2):157–70.

122. Green JD, Narahara H. Assay of succinate dehydrogenase activity by the tetrazolium method: evaluation of an improved technique in skeletal muscle fractions. J Histochem Cytochem. 1980;28(5):408–412.

123. Du J-Z, Du X-J, Mao C-Q, Wang J. Tailor-Made Dual pH-Sensitive Polymer–Doxorubicin Nanoparticles for Efficient Anticancer Drug Delivery. J Am Chem Soc. 2011 Nov 9;133(44):17560–3.

124. Palchaudhuri R, Hergenrother PJ. DNA as a target for anticancer compounds: methods to determine the mode of binding and the mechanism of action. Curr Opin Biotechnol. 2007 Dec;18(6):497–503.

125. Kapuściński J, Skoczylas B. Simple and rapid flourometric method for DNA microassay. Anal Chem. 1977;83(1):252–257.

126. Biswas S, Torchilin VP. Nanopreparations for organelle-specific delivery in cancer. Adv Drug Deliv Rev. 2014 Feb;66:26–41.

7 Appendix

7.1 Appendix A – Protocols

7.1.1 Lactate dehydrogenase activity assay

Lactate dehydrogenase activity assay

Reference: Vassault (1983) Bergmeyer, HU – Methods of enzymatic analysis oxidoreductases and tranferases Vol. 1 P118-126

REQUIRED MATERIALS:

- NADH (Sigma Aldrich – N8129-50mg) Store at -80°C
- TrisBase (Sigma Aldrich - T1503-25G – MW 121.14)
- NaCl (Sigma Aldrich – S3014-500g – MW 58)
- HCl 1M
- Pyruvate (Sigma Aldrich – P5280-25g – MW 110) Store at 4°C

Method:

(A) Prepare **TrisBase/NaCl** stock solution (TrisBase 81.3 mM, NaCl 203.3 mM, pH 7.2):

1. Dissolve 4.92 g TrisBase and 5.95 g NaCl in 400 ml distilled water.
2. Adjust to pH 7.2 at room temperature with 1 M HCl.
3. Make up to 500ml with water.

Stock can be stored at -20°C for at least 12 months.

(B) Prepare **TrisBase/NaCl NADH** solution (TrisBase 81.3 mM, NaCl 203.3 mM, 0.244 mM, pH 7.2):

1. Add 50 mg of NADH to 294 ml of the TrisBase/NaCl stock solution from (A) and mix well.
2. Aliquot into 10 ml stocks and store at -80°C. Samples are stable for at least 12 months. Do not freeze thaw samples.

It is vital to allow the NADH powder to reach room temperature after removal from the freezer. This helps to avoid condensation and formation of inhibitors.

(C) Prepare **TrisBase/NaCl pyruvate** solution (TrisBase 81.3 mM, NaCl 203.3 mM, 9.76 mM pyruvate):

1. Add 10.7 mg of Pyruvate to 10ml of TrisBase/NaCl stock solution from step (A)
2. Aliquot 1 ml into eppendorf tubes and store at -80°C. This solution is stable for up to 2 months.

At the time of the experiment carry out the following assay:

1. Add 250 µl of the TrisBase/NaCl **NADH** solution (B) into a clear 96 well plate.

2. Add 5µl of sample.

3. Place plate on sample holder of plate reader, use mixing function of reader.
4. Allow samples to reach 30°C.

Add 50µl of the TrisBase/NaCl **pyruvate** solution (C) and mix.

Read the initial absorbance at 339 nm and begin timing 30 seconds after mixing.

Monitor decrease in absorbance over 20 minutes with 30 second sampling intervals.

Discard all excess reagents. Do not freeze thaw.

7.1.2 Succinate dehydrogenase standard curve

Protocol - Succinate dehydrogenase standard curve

Reference: Rickwood (1992) Preparative centrifugation. A practical approach. Appendix 4. IRL Press

REQUIRED MATERIALS:

- Iodonitrotetrazolium violet-formazan (Sigma Aldrich I7375, MW 471)
- Dimethylformamide (DMF) (Sigma Aldrich D4551-250ML, MW73)
- Sodium succinate (Sigma Aldrich S5047, MW 270)
- Tris-HCl (Sigma Aldrich T3253 250g, MW 157)
- EDTA disodium salt dihydrate (Sigma Aldrich E5134, MW 372)
- Ethyl acetate 99% (Sigma Aldrich 270989 1l)
- Ethanol 99% (Sigma Aldrich 32221)
- Trichloroacetic acid (Sigma Aldrich T6399 100g)
- HCl
- Homogenisaiton buffer

Stock solutions to be made:

- 10 mM Formazan (INT)
- 200 mM sodium succinate at pH 7.5. This can be stored at -20°C indefinitely.
- 20 mM Tris-HCl (pH 7.4), 0.1 mM EDTA
- Ethyl acetate/ethanol/tricholoracetic acid (5/5/1 ratios)
- 10 mM EDTA
- 1M HCl

Method:

(A) Prepare 10 mM **EDTA**:

1. Dissolve 37 mg of EDTA in 10 ml of distilled water.

(B) Prepare 20 mM **Tris-HCl** 0.1 mM **EDTA** (pH 7.0) buffer:

1. Dissolve 314 mg of Tris-HCl in 80 ml of distilled water.
2. Add 1 ml of EDTA prepared in **(A).**
3. Adjust with HCl to pH 7
2. Make up to 100 ml with distilled water

(C) Prepare 200 mM **sodium succinate** (pH 7.5):

1. Dissolve 5.4 g of sodium succinate in 80 ml of distilled water.
2. Adjust with HCl to pH 7.5
3. Make it up to 100 ml with distilled water.

(D) Prepare 10 mM solution of F**ormazan** in DMF:

1. Dissolve 9.4 mg of formazan in 2ml of DMF for a 10mM solution.

(E) Prepare **ethyl acetate/ethanol/TCA** stopping buffer:

1. Add 50 ml ethyl acetate, 50 ml ethanol and 10 g of TCA.

At the time of the assay, run the following experiment:

1. Prepare the assay mixture:

    I. 5 ml Tris-HCl EDTA buffer **(B)**
    II. 1 ml sodium succinate **(C)**
    III. 1 ml DMF **(D)**
    IV. 20 ml stopping buffer (E)

2. Dilute the 10 mM formazan solution ten fold into assay mixture for a 1 mM solution.
    I. 200 µl into 2000 µl

3. From the 1 mM stock, perform the following dilutions;

Stock number	Stock concentration (mM)	Stock to be used	Stock volume (µl)	Assay mixture volume (µl)
1	1	1	1000	0
2	0.5	1	350	350
3	0.25	1	150	450
4	0.1	1	100	900
5	0.05	4	350	350
6	0.025	4	150	450
7	0.0125	4	75	525
8	0	-	0	1000

4. Plate 200 µl of each sapmle in triplicate in a 96 well plate.

5. Measure the absorbance at 500 nm.

7.1.3 Succinate dehydrogenase assay

Protocol - Succinate dehydrogenase assay

Reference: Rickwood (1992) Preparative centrifugation. A practical approach. Appendix 4. IRL Press

REQUIRED MATERIALS:

- 2-*p*-iodo-phenyl-3-*p*-nitrophenyl tetrazolium chloride (INT) (Sigma Aldrich I10406, MW 505)
- Dimethylformamide (DMF) (Sigma Aldrich D4551-250ML, MW73)
- Sodium succinate (Sigma Aldrich S5047, MW 270)
- Tris-HCl (Sigma Aldrich T3253 250g, MW 157)
- EDTA disodium salt dihydrate (Sigma Aldrich E5134, MW 372)
- Ethyl acetate 99% (Sigma Aldrich 270989 1l)
- Ethanol 99% (Sigma Aldrich 32221)
- Trichloroacetic acid (Sigma Aldrich T6399 100g)
- HCl

Stock solutions to be made:

- 2.5 mg/ml 2-*p*-iodo-phenyl-3-*p*-nitrophenyl tetrazolium chloride (INT)
- 200 mM sodium succinate at pH 7.5. This can be stored at -20°C indefinitely.
- 20 mM Tris-HCl (pH 7.4), 0.1 mM EDTA
- Ethyl acetate/ethanol/tricholoracetic acid (5/5/1 ratios)
- 10 mM EDTA
- 1M HCl

Method:

(A) Prepare 10 mM **EDTA**:

3. Dissolve 37 mg of EDTA in 10 ml of distilled water.

(B) Prepare 20 mM **Tris-HCl** 0.1 mM **EDTA** (pH 7.0) buffer:

4. Dissolve 314 mg of Tris-HCl in 80 ml of distilled water.
5. Add 1 ml of EDTA prepared in **(A).**
6. Adjust with HCl to pH 7
4. Make up to 100 ml with distilled water

(C) Prepare 200 mM **sodium succinate** (pH 7.5):

4. Dissolve 5.4 g of sodium succinate in 80 ml of distilled water.
5. Adjust with HCl to pH 7.5
6. Make it up to 100 ml with distilled water.

(D) Prepare 2.5 mg/ml of **INT** in DMF:

2. Dissolve 5 mg of INT in 2ml of DMF.

(E) Prepare **ethyl acetate/ethanol/TCA** stopping buffer:

2. Add 50 ml ethyl acetate, 50 ml ethanol and 10 g of TCA.

At the time of the assay, run the following experiment:

6. Prepare the incubation mixture in 1.5 ml microcenrifuge tubes:

    I. 250 µl Tris-HCl EDTA buffer **(B)**
    II. 50 µl sodium succinate **(C)**
    III. 50 µl INT **(D)**

7. Start the reaction by adding 50µl of the sample and mix by gently inverting twice.

8. Incubate the mixture at 20-23ºC for 10 minutes. If required run for longer and record the exact time.

9. Stop the reaction by adding 1 ml of stopping buffer **(E)**.

10. Centrifuge for 2 minutes at maximum speed in a microcentrifuge.

11. Remove 200 µl supernatant and place in a 96 well plate.

12. Measure the absorbance at 500 nm.

7.1.4 Alkaline phosphatase activity standard curve

Protocol - Alkaline phosphatase activity standard curve

Reference: D Rockwood (1992) Preparative Centrifugation. A practical approach. Appendix 4

REQUIRED MATERIALS:

- 4-nitrophenol (Sigma Aldrich 1048-5g – MW 139)
- Boric Acid (Sigma Aldrich – B6768-500G, MW 61.83)
- $MgCl_2$ (Sigma Aldrich – M8266-100g, MW 95.21)
- NaOH (Sigma Aldrich – S8045-500g, MW 40)
- Homogenisation buffer

Sock solutions to be prepared:

- 100 mM 4-nitrophenol phosphate. Must be made fresh.
- 50 mM sodium borate buffer (pH 9.8). Stable for months.
- 1.0 M $MgCl_2$
- 1.0 M NaOH
- 0.25 M NaOH

Method:

(B) Prepare **4-nitrophenol phosphate** stock solution:

1. Dissolve 13.9 mg of p-nitrophenol phosphate in 1 ml of Homogenization buffer. (100 mM)

(C) Prepare1.0 M **NaOH** stopping buffer:

1. Dissolve 40 g of NaOH in 900 ml of distilled water.
2. Make up to 1,000 ml with distilled water.

(D) Prepare **boric acid** stock solution:

1. Dissolve 309 mg of boric acid in 90 ml of distilled water. Adjust to pH 9.8 with 1M NaOH.
2. Make up to 100 ml with distilled water.

(E) Prepare **$MgCl_2$** stock solution:

1. Dissolve 952 mg of $MgCl_2$ in 8 ml of distilled water.
2. Make up to 10 ml with distilled water.

(F) Prepare 250 mM **NaOH** stopping buffer:

1. Take 25 ml of 1M NaOH (prepared in **B**), and make up to 100 ml with distilled water.
   Use glass pipette for taking 25 ml of the stock.

(G) Prepare working stock:

1. Mix 5 ml of distilled water with 5 ml of **boric acid (C)** and add 20 µl of **MgCl2 (D)**.

At the time of the experiment carry out the following assay:

5. Prepare the assay mixture by adding 4 ml working stock (F), 1 ml homogenization buffer and 12 ml of NaOH (E) stopping buffer

6. Dilute 4-Nitrophenol into assay mixture one hundred fold, to produce a stock of 1 mM.

7. Dilute this further ten fold, to produce your working stock of 0.1 mM

8. Dilute the mixture in the following manner;

Stock number	Concentration (mM)	Stock number used	Stock volume (µl)	Assay mixture volume (µl)
1	0.11	1	1000	0
2	0.075	1	750	250
3	0.05	1	500	500
4	0.025	1	250	750
5	0.01	1	100	900
6	0	1	0	1000

9. Add 200 µl of each concentration in triplicate into a clear 96 well plate.

10. As a blank use 200 µl of the working stock **(F)**.

11. Measure the absorbance at a wavelength of 405 nm.

7.1.5 Alkaline phosphatase activity assay

Protocol - Alkaline phosphatase activity assay

Reference: D Rockwood (1992) Preparative Centrifugation. A practical approach. Appendix 4

REQUIRED MATERIALS:

- *p*-nitrophenol phosphate disodium salt (Sigma Aldrich 71768-5g - Bis(p-nitrophenyl) phosphate sodium salt, MW 371.14)
- Boric Acid (Sigma Aldrich – B6768-500G, MW 61.83)
- $MgCl_2$ (Sigma Aldrich – M8266-100g, MW 95.21)
- NaOH (Sigma Aldrich – S8045-500g, MW 40)

Sock solutions to be prepared:

- 16 mM *p*-nitrophenol phosphate. Stable at 4°C for 4 weeks.
- 50 mM sodium borate buffer (pH 9.8). Stable for months.
- 1.0 M $MgCl_2$
- 1.0 M NaOH
- 0.25 M NaOH

Method:

(H) Prepare ***p*-nitrophenol phosphate** stock solution:

2. Dissolve 59 mg of p-nitrophenol phosphate in 10 ml of distilled water.

(I) Prepare1.0 M **NaOH** stopping buffer:

3. Dissolve 40 g of NaOH in 900 ml of distilled water.
4. Make up to 1,000 ml with distilled water.

(J) Prepare **boric acid** stock solution:

3. Dissolve 309 mg of boric acid in 90 ml of distilled water. Adjust to pH 9.8 with 1M NaOH.
4. Make up to 100 ml with distilled water.

(K) Prepare **$MgCl_2$** stock solution:

3. Dissolve 952 mg of $MgCl_2$ in 8 ml of distilled water.
4. Make up to 10 ml with distilled water.

(L) Prepare 250 mM **NaOH** stopping buffer:

1. Take 25 ml of 1M NaOH (prepared in **B**), and make up to 100 ml with distilled water.
   Use glass pipette for taking 25 ml of the stock.

(M) Prepare working stock:

1. Mix 5 ml of ***p*-nitrophenol phosphate (A)** with 5 ml of **boric acid (C)** and add 20 µl of **MgCl2 (D)**.

At the time of the experiment carry out the following assay:

12. Add 200 µl of the working stock (p-nitrophenol/boric acid/ $MgCl_2$ **(F)**) into a 1.5 ml Eppendorf tube.
13. Add 50 µl of sample.
14. Incubate the sample at 37˚C for 60 minutes exact.
15. Stop the reaction by adding 600 µl of NaOH stopping buffer **(E).**
16. Centrifuge at 700 g for 20 minutes.
17. Remove 200 µl of the supernatant and place into a clear 96 well plate.
18. As a blank use 200 µl of the working stock **(F)**.
19. Measure the absorbance at a wavelength of 405 nm.
20. Calculate the amount of product formed using a *p*-nitrophenol calibration curve.

7.1.6 N-actyl-β-glucoseaminidase standard curve

Protocol - N-actyl-β-glucoseaminidase standard curve

Klemm et al – 1998 – Effects of polyethylenimineon endocytosis and lysosomal stability – Bio Chem Pharmacology -56 – P 41-46

MATERIALS REQUIRED:

- 4-Methylumbelliferone (Sigma Aldrich – M1381-25MG – MW – 176.17)
- Sucrose (Sigma Aldrich – S9378-500g – MW 342)
- Sodium citrate (Sodium Citrate – Sigma Aldrich W302600-1KG-K – MW 294.7)
- Glycine – NaOH at pH 10.4 (Sigma Aldrich - G7126-500G – MW 75.07)
- 1 M HCl

Stock solutions to be prepared:

- Assay buffer: 5 mM 4-Methylumbelliferyl N-acetyl-β-D-glucosaminide, 250mM sucrose, 200 mM Sodium citrate HCl. Mae up fresh at time of assay.
- 250 mM sucrose
- 200 mM sodium citrate HCl buffer (pH 5.0)
- 250 mM Glycine – NaOH at pH 10.4
- NaOH 1M
- 100 mM 4-Methylumbelliferone

Method:

(A) Prepare 200 mM **sodium citrate – HCl buffer** (pH 5.0):

1. Dissolve 5.88 g of sodium citrate in 80 ml of water make up to 100 ml
2. Adjust pH to 5.0 with HCl 1M
3. Make with distilled water up to 100 ml

(B) Prepare Assay buffer: 250 mM **sucrose /** 200 mM **sodium citrate – HCl buffer** (pH 5.0)

1. Dissolve 855 mg of sucrose in 9 ml of sodium citrate buffer from step (A)
2. Make up to 10ml with sodium citrate buffer (A)

(C) Prepare stopping buffer (250 mM **Glycine NaOH** at pH 10.4)

1. Dissolve 1.87 g Glycine in 80 ml of water
2. Bring to pH 10.4 with 1M NaOH
3. Make up to 100ml with distilled water

At the time of assay perform the following experiment:

4. Add 5 ml of homogenization buffer to 3 ml of assay buffer (B) and 20 ml of Glycine-NaOH stopping buffer

5. Dissolve 17.6 mg of 4–Methumbelferrone in 1ml of methanol

    i. Dilute the above stock 20 fold (200 µl stock into 4ml homogenization buffer), into homogenization buffer to produce a 5 mM solution.
    ii. From this stock produce the following curve

Stock number	Concentration (µM)	Stock used	Stock Volume (µl)	Na Citrate/sucrose buffer (µl)
1	5000	1	1000	0
2	2500	1	500	500
3	1250	1	250	750
4	500	1	100	900
5	250	1	50	950
6	125	1	25	975
7	50	1	10	990
8	25	1	5	995
9	0	-	0	1000

6. USING A BLACK PLATE, place 200 µl of the each sample in a well and measure the florescence of 4-methylumbelliferrone with an excitation wavelength of 360 nm and an emission wavelength of 448 nm.

Notes:

- Free and total activities of the enzyme may be expressed as a percentage.
- For the total activity, run a 100% lysis control using 10% triton.
- This assay can also be used to measure the integrity of lysosomes following fractionation and cell lysis by measuring the free activity of N-actyl-β-glucoseaminidase. Refer to the reference paper for further details.
-

7.1.7 N-actyl-β-glucoseaminidase assay

Protocol - N-actyl-β-glucoseaminidase assay

Klemm et al – 1998 – Effects of polyethylenimineon endocytosis and lysosomal stability – Bio Chem Pharmacology -56 – P 41-46

MATERIALS REQUIRED:

- 4-Methylumbelliferyl N-acetyl-β-D-glucosaminide (Sigma Aldrich - M2133-25MG – MW – 379.3)
- Sucrose (Sigma Aldrich – S9378-500g – MW 342)
- Sodium citrate (Sodium Citrate – Sigma Aldrich W302600-1KG-K – MW 294.7)
- Glycine – NaOH at pH 10.4 (Sigma Aldrich - G7126-500G – MW 75.07)
- 1 M HCl

Stock solutions to be prepared:

- Assay buffer: 5 mM 4-Methylumbelliferyl N-acetyl-β-D-glucosaminide, 250mM sucrose, 200 mM Sodium citrate HCl. Mae up fresh at time of assay.
- 250 mM sucrose
- 200 mM sodium citrate HCl buffer (pH 5.0)
- 250 mM Glycine – NaOH at pH 10.4
- NaOH 1M

Method:

(D) Prepare 200 mM **sodium citrate – HCl buffer** (pH 5.0):

1. Dissolve 5.88 g of sodium citrate in 80 ml of water make up to 100 ml
2. Adjust pH to 5.0 with HCl 1M
3. Make with distilled water up to 100 ml

(E) Prepare Assay buffer: 5 mM **4-methylumbelliferyl N-acetyl-β-D-glucosaminidase** 250 mM **sucrose /** 200 mM **sodium citrate – HCl buffer** (pH 5.0)

1. Dissolve 855 mg of sucrose in 9 ml of sodium citrate buffer from step (A)
2. Add 18.9 mg of 4-methylumbelliferyl N-acetyl-β-D-glucosaminidase
3. Make up to 10ml with sodium citrate buffer (A)

(F) Prepare stopping buffer (250 mM **Glycine NaOH** at pH 10.4)

1. Dissolve 1.87 g Glycine in 80 ml of water
2. Bring to pH 10.4 with 1M NaOH
3. Make up to 100ml with distilled water

(G) At the time of assay perform the following experiment:

1. Add 50 µl of sample to 30 µl of buffer (B) in a 2ml eppendorf tube

2. Incubate for five minutes at 25°C in the dark

3. Stop the reaction by adding 200 µl Glycine NaOH stopping buffer (C)
4. Centrefuge the eppendorf tube at 22,500G for 2 minutes
5. Remove 200 µl of supernatant and place in a BLACK 96 well plate. Protect from light
6. Measure the florescence of liberated 4-methylumbelliferyl with an excitation wavelength of 360 nm and an emission wavelength of 448 nm.

Notes:

- Free and total activities of the enzyme may be expressed as a percentage.
- For the total activity, run a 100% lysis control using 10% triton.
- This assay can also be used to measure the integrity of lysosomes following fractionation and cell lysis by measuring the free activity of N-actyl-β-glucoseaminidase. Refer to the reference paper for further details.

7.1.8 DAPI fluorescent standard curve for DNA

Protocol - DAPI fluorescent standard curve for DNA

Reference: D Rockwood (1992) Preparative Centrifugation. A practical approach. Appendix 4

REQUIRED MATERIALS:

- 4',6-diamidino-2-phenylindole (DAPI) (Roche Diagnostics 1023.627.6001 amount 10 mg)
- EDTA disodium salt dihydrate (Sigma Aldrich E5134 250g, MW 372)
- Tris-HCl (Sigma Aldrich T3253 250g, MW 157)
- NaCl (Sigma Aldrich, MW 58.44)
- DNA standards (Herring sperm DNA, Sigma Aldrich, D7290-1ML)
- HCl
- Black 96 well plates flat bottom (Sigma Aldrich M0312-32EA)
- Homogenization buffer

Stock solutions to be prepared:

- 4 mg DAPI in 100mM NaCl, 10 mM EDTA, 10mM Tris-HCl (pH 7.0). Store stocks at -80°C. Stable for 12 months.

Method:

(A) Prepare DAPI buffer (100 mM NaCl ,10 mM EDTA, 10mM Tris-HCl):

1. Add 58 mg of NaCl, 37 mg EDTA and 15 mg Tris-HCl to 9 ml of distilled water.
2. Adjust to pH 7.0 with 1M HCl
3. Make up to 10 ml with distilled water

(B) Prepare DAPI reagent (working stock 0.1 µg/ml):

1. Add 4 mg of DAPI reagent to 1 ml of DAPI buffer from **(A)** to obtain a 4 mg/ml stock solution.
2. Aliquot 60 µl stock and store at -80°C.
3. Take one aliquot of the DAPI stock and add 50 µl to 2 ml of buffer from **(A)**; mix solution.
4. Perform final dilution by adding 10 µl of the solution to 10 ml of buffer from **(A)** and mixing thoroughly.

(C) Prepare DNA solution

1. Add 2mg of DNA to 1 ml of homogenization buffer. Mix well

Protect sample from light. Wrap working stock in aluminum foil.

At the time of the experiment carry out the following assay:

1. Prepare DNA standards ranging from 2 to 0.1 mg/ml.

Stock number	Concentration (µg/ml)	Stock to use	Stock volume	Homogenisation buffer
1	2000	1	2000	0
2	1000	1	500	500
3	500	1	250	750
4	200	1	200	1800
5	100	4	1000	1000
6	50	5	1000	1000
7	10	5	100	900
8	1	7	100	900
9	0.1	8	100	900

2. Determine the baseline fluorescence for the DAPI solution as a control at an excitation wavelength of 360nm and an emission wavelength of 450nm at 25°C.

3. Use a black 96 well plate. Add 200 µl of DAPI reagent into the required number of wells.

4. Add 20 µl of DNA standard to the well.

5. Read fluorescence as detailed in 1.

Notes:

- Ensure to use same gain is used for samples and standards.
- Protect plate from light; cover with aluminium foil.
- Ensure that all measurements are taken at a uniform temperature.
- Ensure that there are no free cations in the sample as they quenched DAPI fluorescence.
- Use DNA standards with a maximum concentration of 100 µg/ml.

7.1.9 DAPI fluorescent assay for DNA

Protocol - DAPI fluorescent assay for DNA

Reference: D Rockwood (1992) Preparative Centrifugation. A practical approach. Appendix 4

REQUIRED MATERIALS:

- 4',6-diamidino-2-phenylindole (DAPI) (Roche Diagnostics 1023.627.6001 amount 10 mg)
- EDTA disodium salt dihydrate (Sigma Aldrich E5134 250g, MW 372)
- Tris-HCl (Sigma Aldrich T3253 250g, MW 157)
- NaCl (Sigma Aldrich, MW 58.44)
- DNA standards (Herring sperm DNA, Sigma Aldrich, D7290-1ML)
- HCl
- Black 96 well plates flat bottom (Sigma Aldrich M0312-32EA)

Stock solutions to be prepared:

- 4 mg DAPI in 100mM NaCl, 10 mM EDTA, 10mM Tris-HCl (pH 7.0). Store stocks at -80°C. Stable for 12 months.

Method:

(D) Prepare DAPI buffer (100 mM NaCl ,10 mM EDTA, 10mM Tris-HCl):

1. Add 58 mg of NaCl, 37 mg EDTA and 15 mg Tris-HCl to 9 ml of distilled water.
2. Adjust to pH 7.0 with 1M HCl
3. Make up to 10 ml with distilled water

(E) Prepare DAPI reagent (working stock 0.1 µg/ml):

1. Add 4 mg of DAPI reagent to 1 ml of DAPI buffer from **(A)** to obtain a 4 mg/ml stock solution.
2. Aliquot 60 µl stock and store at -80°C.
3. Take one aliquot of the DAPI stock and add 50 µl to 2 ml of buffer from **(A)**; mix solution.
4. Perform final dilution by adding 10 µl of the solution to 10 ml of buffer from **(A)** and mixing thoroughly.

Protect sample from light. Wrap working stock in aluminum foil.

At the time of the experiment carry out the following assay:

6. Determine the baseline fluorescence for the DAPI solution as a control at an excitation wavelength of 360nm and an emission wavelength of 450nm at 25°C.

7. Use a black 96 well plate. Add 200 µl of DAPI reagent into the required number of wells.

8. Add 20 µl of sample to the well.

9. Read fluorescence as detailed in 1.

10. Calculate the DNA content of the sample material with the aid of a calibration curve.

Notes:

- Ensure to use same gain is used for samples and standards.
- Protect plate from light; cover with aluminium foil.
- Ensure that all measurements are taken at a uniform temperature.
- Ensure that there are no free cations in the sample as they will quench DAPI fluorescence.
- Use DNA standards with a maximum concentration of 100 µg/ml.

7.1.10 Preparation of homogenization buffer

Protocol - Preparation of homogenization buffer for subcellular fractionation

REQUIRED MATERIALS:

- Sucrose – (Sigma Aldrich – SO389-500g – MW 342)
- HEPES (Sigma Aldrich – H3375-25g – MW 238)
- EDTA (Sigma Aldrich – EDS 100g – MW 292)
- Aprotinin (Sigma Aldrich – A1153-1MG)
- Pepstatin (Sigma Aldrich – P5318-5MG)
- Leupeptin (Sigma Aldrich – L2884-5MG)
- 1 mM phenylmethanesulfonylfluoride (PMSF, Sigma Aldrich – P7626 – MW 174)

Caution: PMSF is hazardous and highly irritant refer to COSSH.

Complete homogenisation buffer contains:

- 250 mM sucrose
- 1mM EDTA
- 10 mM HEPES
- 2µg/ml Aprotinin
- 1µg/ml Pepstatin
- 2µg/ml Leupeptin
- 1 mM PMSF

METHOD:

(A) Prepare **homogenisation buffer stock** (250 mM sucrose containing 1mM EDTA and 10 mM HEPES):

1. To 150ml of distilled water add 17.11 g of sucrose, 476 mg of HEPES and 58 mg of EDTA. Dissolve and make up to 200 ml.

2. Freeze 10 ml aliquots until required.

(B) Prepare **proteinase inhibitors aliquots** at 1mg/ml concentration:

1. Aprotinin: Add 1ml of water to 1mg of aprotinin in shipping vial and dissolve. Store aliquots at -80°C until use. Stable for at least 6 months when frozen.
2. Leupeptin: Add 1ml of water to 5 mg of leupeptin in shipping vial and dissolve. Transfer 200 µl to eppendorf tubes and add 800 µl of water. Store aliquots at -80°C until use. Stable for at least 6 months when forzen.
3. Pepstatin: Add 1ml of absolute ethanol to 5mg of pepstatin in shipping vial, mix well. Transfer 200 µl to an eppendorf tubes and add 800 µl of absolute ethanol. Mix and store at -80°C until use. Stable for at least 3 months when forzen. Discard when yellow colour develops.

(C) Freshly prepare **PMSF** as it is not stable in water.

1. Add 1ml of absolute ethanol to 17 mg of PMSF and vortex to dissolve.

At the time of the experiment prepare 10 ml of working homogenization buffer:

To **10 ml** of homogenisation buffer stock (prepared in A) add protease inhibitors prepared in (B and C):

1. Add from aprotinnin (1 mg/ml) stock 20 µl
2. Add from leupeptin (1 mg/ml) stock 20 µl
3. Add from pepstatin (1 mg/ml) stock 10 µl
4. Add from PMSF stock 100 µl.

7.1.11 Production of nanoparticles from a silk solution of >5% W/V

Protocol – Production of nanoparticles from a silk solution of >5% W/V

Reference; F P Seib, 2013, 'pH-dependent anticancer Drug Release from Silk Nanoparticles', Advanced healthcare materials.

Required materials

- Silk solution of >5% W/V
- ddH2O
- Acetone

Method

1. Add the silk solution drop wise to acetone maintaining a >75% v/v acetone solution.
2. Centrifuge the silk at 100,000g for 30 minutes
3. Aspirate the supernatant and resuspend the nanoparticles in ddH2O by vortexing for at least 20 seconds
4. Sonicate the resuspension twice at 30% amplitude for 30 seconds.
5. Repeat steps 2 and 3 twice more
6. Following the final centrifugation and resuspension, filter the solution with progressively smaller filters; 5, 0.45 and finally 0.22 µm PVDF filters to yield a uniform suspension
7. Characterize the particles as required according to the significant characteristics.
8. Store at 4C until needed

Notes;

If the current silk solution is of too low a concentration to be used, it can be dialyzed against a 10% PEG solution.

7.2 Appendix B – Conference abstract (NowNano 2014)

Quantitatively tracing the intracellular fate of silk nanoparticles.

S. G. Huff Guelbert* and F.P. Seib

Strathclyde Institute of Pharmaceutical and Biomedical Sciences. 161 Cathedral Street, Glasgow G4 0RE, UK. Sam.huff-guelbert@strath.ac.uk

Silk from the silk worm *B. mori* has long been used as a suture material due to its unmatched mechanical properties [1] excellent biocompatability [2] and degradability *in vivo*. Recently there has be a large effort to use silk for drug delivery applications, for example self-assembling silk hydrogels, films, micro- and nanoparticles for anticancer drug delivery [3]. Nanoparticles are proposed for anticancer drug delivery as they can reach the tumour microenvironment due to leaky vasculature and reduced lymphatic drainage; this phenomenon is known as the enhanced permeation and retention (EPR) effect [4]. The EPR effect permits passive accumulation of nanoparticles. Once nanoparticles reach the tumour microenvironment there is often the need for endocytic uptake and correct intracellular trafficking to yield the desired therapeutic response. We use an acetone desolvation method to generate silk nanoparticles that are uniform in size (100 nm, +/- 10 nm polydispersity), spherical and have a surface charge of -35 mV. However, there is little quantitative data on how silk nanoparticles are trafficked within cells or navigate the tumour microenvironment. We will present quantitative data on the intracellular fate of silk nanoparticles in B16F10 mouse melanoma cells.

References

[1] J Perez-Rigueiro et al., *Journal of Applied Polymer Science*, **2000**, *Vol. 75*, p1270-1277

[2] Y. Yang et al., *Biomaterials*, **2007**, *Vol. 28*, p1643-1652

[3] Seib et at., *Israel Journal of Chemistry*, **2013**, *Vol 59*, 756-766

[4] Y. Matumura and H Maeda, *Cancer Research,* **1986**, *Vol. 46*, p6387-6392